CCL2 blockade combined with PD-1/P-selectin immunomodulators impedes breast cancer brain metastasis

Sahar Israeli Dangoor,[1] Rami Khoury,[1] Koren Salomon,[1] Sabina Pozzi,[1] Shir Shahar,[1] Adan Miari,[1] Yael Leichtmann-Bardoogo,[2] Neta Bar-Hai,[3,4] Neta Frommer,[1] Eilam Yeini,[1] Tom Winkler,[5] Nora Balint Lahat,[6] Iris Kamer,[3] Ori Hadad,[1] Kathrin Laue,[5] Henry Brem,[7] Thomas M. Hyde,[8,9,10] Jair Bar,[3] Iris Barshack,[6,11] Uri Ben-David,[5] Dana Ishay-Ronen,[3,4] Ben M. Maoz[2,12,13,14] and Ronit Satchi-Fainaro[1,12,14]

Abstract

Over the last two decades, the diagnosis and treatment of breast cancer patients have considerably improved. However, brain metastases remain a major clinical challenge and a leading cause of mortality. Thus, a better understanding of the pathways involved in the metastatic cascade is essential.

To this end, we have investigated the reciprocal effects of astrocytes and breast cancer cells, employing traditional 2-dimensional cell culture and our unique 3-dimensional multicellular tumoroid models.

Our findings revealed that astrocytes enhance the proliferation, migration, and invasion of breast cancer cells, suggesting a supportive role for astrocytes in breast cancer outgrowth to the brain. Elucidating the key players in astrocyte-breast cancer cells crosstalk, we found that CCL2 is highly expressed in breast cancer brain metastases tissue sections from both patients and mice. Our *in vitro* and *in vivo* models further confirmed that CCL2 has a functional role in brain metastasis. Given their aggressive nature, we sought additional immune checkpoints for rationale combination therapy. Among the promising candidates were the adhesion molecule P-selectin, which we have recently shown to play a key role in the crosstalk with microglia cells, and the co-inhibitory receptor PD-1, the main target of currently approved immunotherapies. Finally, combining CCL2 inhibition with immunomodulators targeting either PD-1/PD-L1 or P-selectin/P-Selectin Ligand-

1 axes in our human 3-dimensional tumoroid models and *in vivo* presented more favorable outcomes than each monotherapy.

Taken together, we propose that CCL2-CCR2/CCR4 is a key pathway promoting breast cancer brain metastases and a promising target for an immunotherapeutic combination approach.

Author affiliations:

1 Department of Physiology and Pharmacology, Faculty of Medicine, Tel Aviv University, Tel Aviv, 6997801, Israel

2 Department of Biomedical Engineering, Tel Aviv University, Tel Aviv, 6997801, Israel

3 Cancer Research Center, Oncology Institute, Sheba Medical Center, Tel-Hashomer, 5262000, Israel

4 Affiliated with Faculty of Medicine, Tel Aviv University, Tel Aviv, 6997801, Israel

5 Department of Human Molecular Genetics and Biochemistry, Faculty of Medicine, Tel Aviv University, Tel Aviv, 6997801, Israel

6 Department of Pathology, Sheba Medical Center, Tel Hashomer, 5262000, Israel

7 Department of Neurosurgery, Johns Hopkins University School of Medicine, Baltimore, MD 21218, USA

8 Lieber Institute for Brain Development, Johns Hopkins Medical Campus, Baltimore, MD 21218, USA

9 Department of Psychiatry & Behavioral Science, Johns Hopkins University School of Medicine, Baltimore, MD 21218, USA

10 Department of Neurology, Johns Hopkins University School of Medicine, Baltimore, MD 21218, USA

11 Department of Pathology, Faculty of Medicine, Tel Aviv University, Tel Aviv, 6997801, Israel

12 Sagol School of Neuroscience, Tel Aviv University, Tel Aviv, 6997801, Israel

13 Sagol Center for Regenerative Medicine, Tel Aviv University, Tel Aviv, 6997801, Israel

14 The Center for Nanoscience and Nanotechnology, Tel Aviv University, Tel Aviv, 6997801, Israel

Correspondence to: Prof. Ronit Satchi-Fainaro, PhD

Department of Physiology and Pharmacology, Faculty of Medicine, Tel Aviv University, Tel Aviv, 6997801, Israel

E-mail: ronitsf@tauex.tau.ac.il

Running title: CCL2 inhibition hinders brain metastasis

Keywords: breast cancer brain metastasis; 3D cancer models; astrocytes; CCL2; P-selectin; PD-1

Introduction

Breast cancer (BC) is the most common malignancy in women and the leading cause of cancer-related deaths in women worldwide.[1] For locally invasive BC, the 5-year survival rate is above 99%. This rate dramatically decreases to 30% when the disease is spread to distant metastatic sites.[2] BC is one of the main cancer types metastasizing to the brain, with approximately 15% of BC patients developing CNS metastases, presenting an even higher incidence found in autopsies. The survival rate declines even further if the metastatic disease involves the CNS, with a 1-year survival rate of only 20%,[3-5] while suffering from reduced quality of life.[4]

In the last two decades, the diagnosis and treatment of BC patients have considerably improved, including for those at the metastatic stage. However, the incidence of breast cancer brain metastasis (BCBM) is increasing due to earlier detection and longer survival from the primary tumor. Hence, it is still a major clinical problem and a leading cause of death from cancer.[3,4,6,7]

The treatment options for BCBM include stereotactic radiosurgery (SRS), chemotherapy, targeted therapy according to the primary tumor subtype, surgical resection, and whole-brain radiation therapy (WBRT).[8] Unfortunately, the therapeutic benefit of current treatment options is limited.[9]

Thus, it is crucial to gain a better understanding of the pathways that orchestrate the metastatic cascade of BCBM.

In extracranial malignancies, it is well established that the tumor microenvironment (TME) has an essential role in cancer progression and in organ-specific metastasis.[5,10,11] In recent years, it has become clear that the unique brain tumor microenvironment (bTME) also plays a role in the pathology of primary and metastatic brain tumors.[12-15] Data regarding specific therapeutic targets in BCBM has started to be gathered in recent years,[16-18] and the involvement of the bTME in BCBM development and progression is beginning to be evident.[19-22]

Brain tumors in both animal models and in patients usually encompass reactive astrocytes.[23-26] Astrocytes are responsible for brain homeostasis, and they do not proliferate in normal adult brains. However, in response to brain injury, astrocytes can be activated, leading to astrogliosis and glial scar formation. Similarly, brain metastases (BM) are also inducers of local activation of astrocytes, neuroinflammation, and astrogliosis.[13,27] Furthermore, astrocytes can support the formation and progression of BM, by communicating with the cancer cells *via* secreted factors, e.g., cytokines, enzymes, and neurotrophic factors, and the inhibition of such factors can lead to prevention or regression of BM depending on the disease stage.[15,28,29]

Activated microglia are also often found nearby and within brain tumors.[24,30-33] Microglia are macrophages-like cells and serve as the brain-resident immune cells. They play diverse roles in cancer, which could be attributed to their heterogeneity and the different activation states.[28] Microglial cells can lead to cancer-promoting effects by secretion of factors such as cytokines, growth factors, and enzymes,[12,24,32,34,35] and glioma proliferation can be attenuated by the inhibition of microglial activation.[30] On the other hand, it has also been reported that microglia can elicit cytotoxicity against BM from lung cancer.[36]

These findings demonstrate that upon arrival to the brain, extensive direct and indirect crosstalk between the brain resident cells and tumor cells occur, resulting in a multitude of pathway activations, both in tumor and host cells. Furthermore, the tumor cells that succeed in colonizing the brain appear to have gained the ability to exploit brain endogenous substrates that are naturally secreted by the resident cells as oncogenic signals.[37] Understanding the contribution of interactions between metastatic BC cells and host bTME cells to brain metastasis colonization may provide a novel therapeutic approach to prevent BM formation.

Here, we show that via secretion of CCL2, astrocytes support BCBM by enhancing the tumorigenic properties of BC cells, such as proliferation, migration, and invasion. CCL2 (also known as monocyte chemoattractant protein-1/MCP-1) is a low molecular weight cytokine with chemoattractant activity (i.e., chemokine),[38] and CCR2 and CCR4 are the receptors that are known to bind it.[39] Additional promising targets for combination therapy are the adhesion molecule P-selectin (SELP) and its ligand (PSGL-1), and the co-inhibitory receptor programmed cell death protein-1 (PD-1) and its ligand (PD-L1). We have recently shown that the SELP-PSGL-1 axis is involved in glioblastoma-microglia crosstalk and is a key regulator of glioblastoma progression.[40] Additionally, immunotherapies are becoming reasonable treatment options, as the involvement of the immune system in BC progression has recently been re-evaluated.[41] In melanoma and non-small cell lung cancer (NSCLC) BM, targeting PD-1 or PD-L1 has already been shown to have intracranial efficacy.[42,43] Collectively, our findings outline the CCL2-CCR2/CCR4 axis as a key player in astrocyte-BC cells crosstalk during the BCBM cascade, and offer a potential new immunotherapeutic combination approach for this devastating disease.

Materials and methods

Breast cancer 3D tumor spheroids

Multicellular tumor spheroids were prepared using a modification of the hanging-drop method[44], in which droplets of cell suspension are held hanging from the bottom of an inverted tissue-culture plate until cells agglomerate spontaneously at the lower part of the droplet due to gravity. The full details can be found in the supplementary materials and methods.

BBB Co-culture and BBB-Chip with astrocytes and MDA-MB-231 cells

The experiments were done in two formats: Commercial 24-well Transwell® (Costar Corp., Corning, NY, USA ing) and BBB-Chip platform (Supplementary Fig. S16A) that was fabricated as previously described[45,46]. For both platforms, the BMEC were seeded as mentioned in the supplementary materials and methods. The following day, the underpart of the membrane was coated with 3% Matrigel for 1 hour, then human primary astrocytes (ScienCell, 1800-scl) were seeded at a ratio of 1:2 astrocytes: BMEC. Astrocytes were incubated for at least an hour before

flipping the membrane into the BMEC well containing endothelial serum-free medium supplemented with B27 and 100 U/ml Penicillin, and 100 µg/ml Streptomycin. Human primary brain vascular pericytes (ScienCell 1200-scl) were seeded on top of BMEC layer at a ratio of 1:3 pericytes: BMEC. Barrier function was evaluated by TEER measurements (Millicell ERS-2 Voltohmmeter, Merck Millipore) daily.

mCherry-labeled MDA-MB-231 cells ($1x10^5$) were added to the upper side of the Transwell®, and treated with 0.3 mM Bindarit, 1 µg/ml CCL2 or with no treatment, as control. TEER values were followed up to 24 hours after MDA-MB-231 cells administration. Cells on Transwells® were then fixed with 4% Paraformaldehyde (PFA) for 10 minutes, following Dulbecco's Phosphate Buffered Saline (PBS) washes, and immunostaining.

Gene expression analysis

Gene expression data were downloaded from the Gene Expression Omnibus database https://www.ncbi.nlm.nih.gov/geo/ (accession number GSE12276). mRNA expression levels of CCL2 (216598_s_at), CCR2 (206978_at), CCR4 (208376_at), SELP (206049_at), SELPLG (209879_at), CD274 (223834_at), and PDCD1 (207634_at) were compared between primary tumors that relapsed to the brain and breast tumors that relapsed to other distant organs, using a one-tailed non-paired Student's t-test.

3D Tumor spheroids for drug combination

For assessing the effect of immunotherapeutic drug combinations, Multicellular tumor spheroids were prepared using the liquid overlay technique[47], in which cell suspension is seeded in Round Bottom Ultra-Low Attachment Microplates, and the cells agglomerate spontaneously at the lower part of the well due to gravity. The full details can be found in the supplementary materials and methods.

Breast cancer 4T1 intracranial animal model

To generate primary BC prior to BCBM, 4T1 cells ($3x10^5$ cells/100 µL) were inoculated into the mammary fat pad of immunocompetent 8-week-old female BALB/c mice (Envigo, CRS). Tumor growth was measured using a caliper, and the tumor volume was calculated using the standard formula: length × $width^2$ × 0.52. Once they reached a volume of 70 mm^3, the primary lesions were

resected. For drug efficacy studies, 4T1 cells ($2x10^4$ cells/2 µL) were stereotactically inoculated into the striatum (2 mm left from the bregma and 3.5 mm depth) of the same mice (previously bearing the primary tumor). Three days following cell inoculation, mice were treated intravenously (i.v.) with 100 mg/kg bindarit or the corresponding vehicle every other day (QOD), i.v. with 16 mg/kg SELPi or the corresponding vehicle QOD, and intraperitoneally (i.p.) with 10 mg/kg Anti-Mouse PD-1 In Vivo Antibody or PBS twice a week. Fourteen days post BC cells intracranial inoculation, 4 mice per group were euthanized, blood was collected, and mice were immediately perfused with 4% PFA in PBS. Brains were then harvested for further immunostaining analysis. Mouse body weight was monitored three times a week, and tumor growth was followed twice a week using 4.7 T/1 H MRI. Mice were euthanized when they lost 10% body weight in a week, had lost 20% of their initial weight, or when neurological symptoms appeared.

Randomization and assignment of mice to the treatment groups

In order to avoid bias in the results, before starting the treatments, all mice were randomly assigned to one of the treatment groups.

Human specimens

FFPE breast cancer samples (brain metastasis, *n*=36; primary breast cancer, *n*=18, adjacent breast tissue, *n*=5), FFPE lung cancer samples (brain metastasis, *n*=26; primary lung cancer, *n*=17, normal lung tissue, *n*=6), and frozen PBMCs from healthy donors (*n*=10) were obtained from Sheba Medical Center following an informed consent. The manipulation of the human samples for immunostaining was accepted by the ethics committees of Tel Aviv University and Sheba Medical Center, under an approved IRB (5727-18-SMC) protocol. Healthy human brain samples were collected by Thomas Hyde at the Lieber Institute for Brain Development as described under an approved IRB protocol, 90-M-0142.

Statistical analyses

Data are expressed as mean ± standard deviation (SD) for *in vitro* assays, or ± standard error of the mean (SEM) for *in vivo* and *ex vivo* assays. Unless otherwise stated, statistical significance was determined using an unpaired, two-sided t test when comparing between two groups, and multiple comparisons ANOVA test when comparing more than two groups. $P < 0.05$ was considered

statistically significant. For Kaplan–Meier survival curves, p. values were determined using a log-rank survival analysis test, with further adjustment of P-values using Holm-Šídák analysis. Statistical analysis was performed using GraphPad Prism 10 (GraphPad Software, Boston, MA).

No statistical method was used to predetermine the sample size. Still, the sample size was chosen to be adequate to receive significant results as determined by preliminary experiments and based on previous publications of multiple groups in the field.[19,48-50]

Results

Astrocytes and BC cells crosstalk result in enhanced proliferation, migration, and invasion

Aiming to evaluate the role of astrocytes in BCBM progression, we utilized both traditional 2-dimensional (2D) co-culture and 3-dimensional (3D) multicellular cancer models. In line with previous reports on the tumorigenic effect of astrocytes on MDA-MB-231 breast cancer cells,[51] our investigations revealed that both murine and human mammary adenocarcinomas, 4T1 and MDA-MB-231 cells, respectively, present increased proliferation rates when co-cultured with primary astrocytes, in a dose-dependent manner (Fig. 1A-B). The relevance of the selected cell ratios was confirmed by analysis of GFAP-positive astrocytes in the vicinity of the tumor region, in an *in vivo* EMT6 mouse model. Staining and analyzing cell ratios revealed there are 1.657 more astrocytes than cancer cells in the tumor area (Supplementary Fig. S1), suggesting that the range of ratios of 1:1 and 1:2 that we selected are physiologically relevant. The higher cell ratios (1:3, 1:4, 1:5), clearly show the dose-dependent effect that astrocytes have on breast cancer proliferation.

In addition, the presence of 4T1 conditioned medium (CM) or MDA-MB-231 CM, which contains cancer cell-secreted factors, increased the proliferation rates of murine and human astrocytes, respectively (Fig. 1C-D). Using a transwell® migration assay, we found a significant increase in 4T1 cell migration towards murine primary astrocytes (mAstro), and in MDA-MB-231 cell migration towards human primary astrocyte (hAstro) CM (Supplementary Fig. S2A-B). The same effect was found with another murine BC cell line, EMT6, which is BRCA-mutated (Supplementary Fig. S2C).

We further characterized the mutual interactions between BC cells and the brain metastatic niche in a 3D model to better mimic the bTME. To that end, we established a 3D multicellular BCBM spheroid model containing BC cells, astrocytes, and brain endothelial cells, separately or combined. These spheroids are created using a modified hanging drop method[44] and later transferred into Basement Membrane Extracts (BME). Utilizing this model, by monitoring the 3D spheroids using live imaging (based on the fluorescence signal of the BC cells), we could assess the proliferation, migration, and invasion of the BC cells.

Supporting the results obtained from the classic 2D culture assays, we identified a significant increase in the growth and sprouting of BC cells in 3D BCBM spheroids containing astrocytes, compared to spheroids containing BC cells only (Fig. 1E-H). In addition, the presence of the Blood-Brain Barrier (BBB) human cerebral microvascular endothelial cells (hCMEC/D3) increased MDA-MB-231 3D spheroid growth and sprouting (Supplementary Fig. S2D-E).

As an additional model of the bTME, we created an advanced BBB model composed of induced pluripotent stem-cell (iPSC)-derived brain microvascular endothelial cells (BMEC), primary human pericytes (optional), and hAstro, using both Transwell® and BBB-Chip[45,52] platforms. We monitored the trans-epithelial electrical resistance (TEER) values until the impedance was above 1000 Ω*cm^2, indicating a good barrier function, before starting the experiments. Interestingly, the addition of astrocytes increased the TEER values, indicating a tighter barrier, while the addition of MDA-MB-231 cells hampered the barrier, indicated by lower TEER values (Fig. 1J). As expected, the transmigration of MDA-MB-231 cells through the barrier lacking any cells, towards astrocytes, was much faster than the transmigration through the BMEC barrier (Fig. 1I, Supplementary Mov. S1-2). The addition of astrocytes to the endothelial system significantly increased MDA-MB-231 trans-endothelial migration, which also occurred faster compared to the BMEC-only barrier (Fig. 1I, Supplementary Mov. S2-3). This shows that although astrocytes enhance the barrier integrity, their crosstalk with BC cells resulted in increased trans-endothelial migration.

CCL2-CCR2/4 axis is upregulated in BCBM

Following the elucidation of the reciprocal effects between astrocytes and BC cells, we aimed to identify secreted factors involved in this intercommunication. Therefore, we performed cytokine arrays on 4T1 cells co-cultured with mAstro and MDA-MB-231 cells co-cultured with hAstro, in which a set of upregulated cytokines was found (Fig. 2A-B, and Supplementary Fig. S2A-B). We

identified CCL2 as one of the factors that are secreted at an exceptionally high level in the co-culture conditions, and it was upregulated both in the human and the murine models (Fig. 2A-B, and Supplementary Fig. S3A-B).

Taken together, we decided to focus on the role of CCL2-CCR2/CCR4 axis in BC-astrocytes interactions. The expression of these markers was validated on tissue sections from 4T1 BCBM mouse model. First, we injected 4T1 cells orthotopically into the mammary fat pad of immunocompetent female BALB/c mice, and following surgical removal of the primary tumor, we performed intracranial cell injection to the same mice. Resembling the expression levels found in humans, all 3 markers, CCL2, CCR2, and CCR4, presented high levels in the mice BM, in comparison to the primary tumors and normal breast and brain tissues (Fig. 2C, E-G). The presence of these three markers was also confirmed in BM of a spontaneous model of intracardially injected EMT6 cells (Supplementary Fig. S6A-B). To verify the clinical relevance of these findings, we validated the expression of CCL2, CCR2, and CCR4 by immunohistochemistry (IHC) staining of formalin-fixed paraffin-embedded (FFPE) clinical samples of BCBM. We found that CCL2 and CCR2 are highly overexpressed in BM and primary BC, compared to normal breast and normal brain tissues (Fig. 2D, H-I). Even though CCR4 presented generally lower expression levels than CCR2, it was also overexpressed in the BM samples (Fig. 2D, J). We further analyzed the expression levels using data from primary tumors of BC patients that later on metastasized to the brain or to other organs (GSE12276).[53] Although not reaching statistical significance, all 3 markers, CCL2, CCR2, and CCR4, showed a trend towards higher expression in the tumors that later on metastasized to the brain (Fig. 2K-M).

To further validate the expression of CCL2, we performed ELISA assays measuring the protein secretion level. In agreement with our findings derived from the cytokine arrays, higher secretion of CCL2 was demonstrated when 4T1 or MDA-MB-231 cells were co-cultured with astrocytes, compared to the respective mono-cultures (Fig. 3A-B).

To reveal the main source of CCL2, we further validated the mRNA expression level of CCL2 using RT-qPCR. 4T1 cells and mAstro were grown in each other's CM, astrocyte starvation medium (0% serum), or full astrocyte medium. mCherry-labeled MDA-MB-231 cells and iRFP-labeled hAstro were mono- or co-cultured, and then sorted by their fluorescence. We found that the activation with starvation medium increased CCL2 expression by mAstro, and when cultured

in 4T1 CM, mAstro CCL2 expression was further increased (Fig. 3C). When MDA-MB-231 and hAstro were co-cultured, the astrocytes expressed much higher levels of CCL2, compared to the monocultures (Fig. 3D). These findings indicated that astrocytes are the main source of CCL2 secreted in the astrocyte-BC cell crosstalk.

To validate the activation state of the astrocytes which are the main source of the secreted CCL2, we performed a FACS analysis. We exposed murine astrocytes to either 4T1 serum-free medium (SFM) (negative activation), 4T1 SFM supplemented with lipopolysaccharide (LPS) (positive activation), or 4T1 CM, and tested the resulting expression of intracellular CCL2 in two types of astrocytic populations: (i) activated / reactive astrocytes (GLAST negative, GFAP positive), and (ii) non-GFAP activated astrocytes (GLAST positive, GFAP negative cells). Our results revealed that non-activated astrocytes (GLAST+GFAP-) generally express much less CCL2 than the activated astrocytes (GLAST-GFAP+), and the different activation media have influenced the level of CCL2 expression by the activated astrocytes (Fig. 3E-F). The exposure of mAstro to breast cancer cell-secreted factors from the 4T1 CM, induced the highest CCL2 expression by the activated astrocytes in the culture (Fig. 3E).

In addition, we assessed the expression levels of the receptors for CCL2 by flow cytometry. CCR2 and CCR4 were both found to be expressed on the surface of 4T1 and MDA-MB-231 cells. When activated with a starvation medium, both cell lines presented an increased level of CCR2 and CCR4, with a further increase when cultured in astrocyte CM (Fig. 3G-N).

As melanoma, breast, and lung cancer are the leading three primary tumor sites metastasizing to the brain,[5] and we have previously established the importance of CCL2 in the context of melanoma brain metastasis,[15] we decided to search for evidence that the CCL2 pathway is important for brain metastatic process in general, and not limited to breast cancer only. Thus, we investigated this phenomenon also in lung cancer brain metastasis.

We characterized lung cancer brain metastases specimens by IHC, of both clinical samples and our mouse models. The immunostaining analysis revealed that CCL2, CCR2, and CCR4 are highly expressed in primary lung cancer (Supplementary Fig. S12A-B and Supplementary Fig. S13A-B) and in lung cancer brain metastases (Supplementary Fig. S12C-D and Supplementary Fig. S13C-D), compared to the corresponding normal tissues. Interestingly, the change in CCL2 expression of BM compared to normal brain was 2-fold higher than that of its primary counterpart, 1.2-fold

for CCR2, and 20-fold for CCR4. Both astrocytes and microglia were found to be activated in the human and murine specimens of lung cancer brain metastases, indicated by GFAP and Iba1 markers, respectively (Supplementary Fig. S12C-D and Supplementary Fig. S13C-D).

The CCL2-CCR2/CCR4 axis is paramount for BC cell proliferation, migration, and invasion

In order to evaluate the role of CCL2 in the crosstalk between BC cells and astrocytes, we performed proliferation, migration, and 3D spheroids experiments in the presence of a CCL2 small molecular-weight inhibitor, bindarit. First, we performed proliferation assays of 4T1 and MDA-MB-231 cells, co-cultured with astrocytes or mono-cultured. In both cases, when the cells were treated with bindarit, BC cell proliferation dramatically decreased, mainly in the co-cultures, bringing it back to similar levels as in the mono-cultured cells that were not treated with the drug (Fig. 4A-B). A similar effect was achieved using a CCL2 neutralizing antibody (Supplementary Fig. S4A-B). In addition, using a Transwell® migration assay, recombinant CCL2 protein (rCCL2) significantly increased MDA-MB-231 migration (Supplementary Fig. S4C), and the inhibition of CCL2 by bindarit significantly decreased MDA-MB-231 cell migration towards hAstro CM (Supplementary Fig. S4D). We further performed 3D tumor spheroids experiments, containing either BC cells alone, or BC cells and astrocytes. When we treated the astrocyte-containing spheroids with bindarit, we observed a significant decrease in spheroid growth and sprouting (Fig. 4J-M). Similar results were obtained by using CCL2 neutralizing antibody, on astrocyte-containing MDA-MB-231 or EMT6 spheroids (Supplementary Fig. S4E-F).

We have also created CCR4 KD cell lines using shRNA in order to molecularly inhibit this pathway. We performed proliferation assays in the presence of astrocytes. 4T1 shCCR4 and MDA-MB-231 shCCR4 both presented a reduced proliferation rate when co-cultured with astrocytes (Fig. 4C-D). The shCCR4 cells proliferation rate was very similar in the presence or absence of the astrocytes (Fig. 4C-D), confirming that the astrocytes' proliferative-promoting effect on the BC cells was mainly mediated by the CCL2 pathway.

Utilizing our BBB model, the inhibition of CCL2 by bindarit has led to a significant increase in the TEER values (Fig. 4H), and in the expression of the tight junction marker ZO1 (Fig. 4I), both indicating a tighter barrier. As expected, the addition of rCCL2 to the barrier has led to a decrease

in the TEER values (Fig. 4G), indicating a loose barrier. Moreover, rCCL2 treatment has led to a more diffuse ZO1 pattern that relocated from the membrane to the cytoplasm (Fig. 4I).

Utilizing our lung cancer models, we observed an increased proliferation rate of both human and murine lung cancer cells, A549 and LLC, respectively, in the presence of astrocytes, which was attenuated by the inhibition of CCL2 using bindarit (Supplementary Fig. S14A-B). Similar effect was detected using 3D multicellular lung cancer brain metastases model (Supplementary Fig. S14C-D). Lastly, we utilized our lung cancer brain metastases mouse model for an efficacy study of bindarit. By inhibiting CCL2, bindarit has led to a significant reduction in BM volume, measured by MRI, compared to the control group (Supplementary Fig. S15A-B).

P-selectin-P-selectin ligand-1 and PD-1-PD-L1 axes are upregulated in BCBM

Most oncology protocols require the need for combination therapy, in order to allow synergistic activity as well as increased therapeutic index of drugs with distinct mechanisms of action, improved toxicity profiles, and prevention of mechanisms of acquired resistance.[54] As we consider the CCL2-CCR2/CCR4 axis to be an immunological target, we rationally sought additional immune checkpoints to combine with CCL2 inhibition therapy. Therefore, we focused on SELP-PSGL-1[12] and PD-1-PD-L1[55] axes.

We performed IHC staining on tissue sections, by which we validated the expression of SELP and PSGL-1. We found both proteins to be upregulated in BCBM compared to their expression in primary tumors and normal brain tissues, both in clinical samples and in our mouse model (Supplementary Fig. S5A-C). Further validation on patient data from GSE12276 dataset[53] also showed a significantly increased expression of SELP and PSGL-1 in primary tumors that metastasized to the brain compared to tumors that metastasized to other organs (Fig. 5A-B).

We validated the expression of PD-1 and PD-L1 by IHC staining of 4T1 BCBM mouse model. We found that both PD-1 and PD-L1 are upregulated in BCBM compared to primary tumors, and normal breast and brain tissues (Supplementary Fig. S5B-C). Validation on patient data from GSE12276 dataset[53] confirmed that both PD-1 (significantly) and PD-L1 (non-significantly) present higher levels of expression in primary BC tumors that metastasized to the brain compared to BC tumors that metastasized to other organs (Fig. 5C-D).

The presence of SELP, PSGL-1, PD-1, and PD-L1 was further confirmed in BM of a spontaneous model of intracardially injected EMT6 cells (Supplementary Fig. S6).

Inhibition of CCL2 with SELP or PD-1-PD-L1 inhibition leads to improved outcomes versus monotherapy

Finally, we tested the inhibition of CCL2, SELP, and PD-1/PD-L1, each alone or combined, using 3 different models: (i) 3D multicellular BCBM spheroid model, (ii) 3D patient-derived metastatic BC organoids co-cultured with bTME milieu, and (iii) immunocompetent BALB/c mouse model.

As a human model for testing the drug combinations, we designed a unique 3D multicellular BCBM spheroid model, which is clinically-relevant. This model enables us to explore immunotherapies, which is not possible with human cell lines or patient-derived xenografts (PDX) injected or implanted into mice, respectively, as these require immunocompromised animals. Therefore, we developed this additional model, which, unlike the model previously described above, is composed of BC cells, astrocytes, and microglia, surrounded by PBMCs.

Prior to *in vivo* studies, utilizing this model, we found that the inhibition of either CCL2, SELP, or PD-L1, each as a monotherapy has led to a reduction in the spheroid growth (Fig. 5E-G). The combination of CCL2 inhibitor with either PD-L1 inhibitor (PD-L1i) or SELP inhibitor (SELPi), both led to a further reduction in spheroid growth (Fig. 5E-G).

As an additional model to test these combination therapies, we utilized patient-derived metastatic BC 3D organoids, and cultured them together with astrocytes, microglia, and PBMCs. By immunostaining the organoids with Cytokeratin 14 (CK14) as a marker for BC cells, we were able to quantify the effect of the treatments on organoid growth (Fig. 5H-J, and Supplementary Fig. S7). The analysis has revealed that the organoids were highly sensitive to the treatment with bindarit as a monotherapy (Fig. 5I-J). We further treated this model with SELPi, PD-L1i, and the clinically used αPD-1 antibody, Pembrolizumab. The combination of bindarit with either of these 3 drugs, was better than these drugs alone, though not superior to bindarit alone (Fig. 5I-J).

To model the disease course *in vivo*, as closely as possible to the human disease in which metastases develop only after a primary tumor was established, 4T1 cells were first inoculated orthotopically into the mammary fat pad, and tumors were later resected. The existence of a primary tumor, is also necessary in order to achieve an intracranial response to immune checkpoint

inhibitor (ICIs), as previously shown in a melanoma BM model.[56] To make sure that there are no metastases present at the stage in which we removed the primary tumor, the resection of the primary tumors was done when they reached very small tumor volume (<50 mm^3), unlikely to have already metastasized. The tumors had well-defined edges and were removed as a whole, as shown by the H&E representative slides (Supplementary Fig. S8). To evaluate the therapeutic effect of anti-cancer drugs, it was important to have a model with 100% brain metastases development that allows for follow-up and monitoring using MRI, in order to show the effect of the drugs on metastases progression. Thus, following the resection of the primary tumor, 4T1 cells were injected intracranially, and mice were treated with the drugs for two weeks: CCL2 inhibitor bindarit, SELPi, and αPD-1 antibody. The experiment time course and treatment regimen are detailed in Fig. 6A.

Each of the drugs significantly increased mice overall survival (OS), compared to the control group. Combining bindarit with either of the other targets has led to a further increase in OS (Fig. 6B-C). Analysis of the systemic disease relapse, presented by primary tumor recurrence or detection of extracranial metastases, revealed another advantage of the combination therapies. While bindarit and SELPi each alone did not show any improvement in relapse in comparison to the control group, the combination of both drugs demonstrated a delay in the detection of any relapse, and a decrease in the overall percentage of mice presenting extracranial metastases or tumor recurrence (Fig. 6D). In the case of the ICI, αPD-1 antibody had a better profile regarding mice relapse compared to the control group, and when combined with bindarit, this was even further improved (Fig. 6E). These findings suggest that combinations with inhibitors of the CCL2-CCR2/CCR4 axis may also impede recurrence and other extracranial metastases besides the BM.

No additional toxicities were detected due to the combination of two drugs, either by body-weight changes (Fig. 6H), or by blood chemical and hematological tests (Supplementary Fig. S9-10).

Each of the drugs alone has also led to a significant decrease in BM volume (Fig. 6F-G). Both of the drug combinations have led to a further non-significant slight improvement compared to the monotherapies (Fig. 6F-G).

Mice brain tissues were collected and further analyzed by IHC staining (Fig. 7, and Supplementary Fig. S11). The analysis revealed that all treatments have led to lower levels of CCL2, CCR2, and CCR4, indicating decreased inflammation. In addition, inhibition of proliferation was observed as

indicated by the proliferation marker Ki-67, together with increased apoptosis indicated by the Caspase-3 marker. Blood vessel density was strongly reduced by bindarit, and even further reduction was presented following the combination treatments, indicated by CD31 marker. As expected, CD8+ cytotoxic T lymphocyte infiltration was increased by all treatment options, either monotherapies or combination therapies. The expression of CD4+ T helper cells did not change significantly between the groups. The presence of FOXP3+ regulatory T cells (Treg) was slightly decreased by all treatments (non-significantly), and the combination of bindarit and αPD-1 treatment presented lower levels of Treg cells. The expression levels of PD-L1 were reduced when the mice were treated with either SELPi, αPD-1 antibody, or the drugs' combinations. This could be due to an effect of the drugs on the antigen-presenting cells (APC), such as dendritic cells or macrophages, pushing them towards a pro-inflammatory M1-like phenotype. The reduced PD-L1 expression and the pro-inflammatory activation of myeloid cells led to a reduction in their immunosuppressive effect on the cytotoxic T cells, resulting in a lower expression of PD-1.

Discussion

CCL2 is a critical proinflammatory cytokine in cancer, as it mediates the signaling of both CCR2 and CCR4.[57] Therefore, this signaling axis has drawn considerable attention in the cancer research field.[57-62] Previous studies have largely focused either on the correlation of CCL2 expression with BC histological grade[63] or on its important role as a regulator of angiogenesis and immune cell recruitment.[64-66] Moreover, CCL2 has been further shown to promote extracranial metastasis by supporting BC cell proliferation, survival, migration, and invasion.[67-72] However, the pro-metastatic effects of the bTME induced by astrocyte-secreted CCL2 are largely unknown.

We have characterized the mutual effects of astrocytes and BC cells in co-cultures and in the presence of CM, mimicking the settings in the different steps of metastases formation, from distant communication to physical interactions. Our findings confirm a reciprocal activation of astrocytes and BC cells, suggesting that reactive astrocytes can remotely facilitate BC cell migration. We developed an additional model for mimicking the clinical scenario, in which BC cells extravasate from the bloodstream into the brain through the BBB, which is demonstrated by the trans-endothelial and trans-astrocytic passage towards astrocyte-secreted cytokines. This model also revealed that even without physical interactions, astrocytes enhanced BC cell penetration through the BBB model. Once the BC cells penetrate the brain parenchyma, their proliferative and

invasiveness abilities are induced by astrocytes. Collectively, our results suggest that astrocytes have a supportive role in the metastatic process of BC in the brain.

We further identified some cytokines as candidates involved in BC-bTME interactions. The leading candidate was CCL2, which was not only found to be overexpressed in co-cultures of BC cells and astrocytes but was also found to be highly relevant in clinical samples, as we showed that it was overexpressed in BM compared to primary tumors and normal breast and brain tissues.

Cancer and stromal cells in the TME can produce CCL2, which affects cancer cells directly and indirectly by recruitment of pro-tumorigenic host stromal cells during metastasis (including, among others, tumor-associated macrophages (TAMs), Tregs, and myeloid-derived suppressor cells (MDSCs)).[39,57,73,74] The stromal expression of CCL2 was found to correlate with relapse-free survival.[75] The receptors that are known to bind CCL2 are CCR2 and CCR4. CCR2 expression was found to promote the recruitment of TAMs at the primary tumor and to enhance invasion, angiogenesis, and extracranial metastasis of breast cancer.[73] CCR4 expression has a strong correlation to lower overall survival in breast cancer patients, and also positively correlates with tumor recurrence and lymph node, lung, and bone metastasis.[74] As far as we know, prior to our publication regarding melanoma BM, the key role of CCL2-CCR2/CCR4 axis has not been shown in the context of astrocyte-cancer cells crosstalk.[15]

In the case of BCBM, we are now showing that the main source of the secreted CCL2 is the activated astrocytes that support the tumorigenic properties of the cancer cells. The BC cells, in turn, increase the expression of CCR2 and CCR4. When we functionally neutralized the CCL2-CCR2/CCR4 axis, either pharmacologically or molecularly, BCBM cell proliferation, migration, and invasion rates decreased, and BBB integrity was improved. To the best of our knowledge, this is the first report demonstrating that activated astrocytes play a key role in BCBM *via* secretion of CCL2, interacting with CCR2 and CCR4 on the surface of BC cells.

We are suggesting that the CCL2 pathway is important for the metastatic colonization process in the brain in general and is not limited to breast cancer only. To strengthen the evidence supporting our hypothesis, we are also showing the CCL2-CCR2/CCR4 axis contribution to lung cancer BM in several models. As we have previously established the importance of this axis in the context of melanoma BM,[15] and are now showing evidence for its role in BCBM and in lung cancer BM, we suggest that CCL2-CCR2/CCR4 axis is a key pathway in the brain metastatic cascade arising from

the leading three primary tumor sites metastasizing to the brain.[5] We further propose that the CCL2 pathway plays a key role in astrocyte-cancer cell signaling during BM formation. We hypothesize that this is an interesting phenomenon, where different types of cancer cells arising from different origins and locations may share a common signaling pathway to interact with astrocytes and lead to brain metastases colonization, establishment, and progression.

As BM are highly aggressive, monotherapy is usually ineffective, and tumor resistance mechanisms can elicit disease relapse.[76] Specifically, CCL2 inhibition in metastatic BC mouse models has been reported to increase metastatic relapse, after cessation of the treatment.[77] Therefore, we decided to search for additional targets to be combined with CCL2 inhibition. We decided to seek targets involved in the interactions with additional bTME components.

In our previous study, we reported the expression of SELP on glioblastoma cells to modulate the activation state of microglia and influence T-cell recruitment.[40] We further characterized the P-selectin–P-selectin ligand-1 axis as a key regulator of the crosstalk between glioblastoma and microglial cells, and demonstrated a potential therapeutic approach for glioblastoma.[40] The inhibition of SELP led to reduced tumor growth and increased survival in glioblastoma mouse models.[40]

ICIs targeting PD-1 or its ligand PD-L1 have demonstrated intracranial effects in brain metastases originating from melanoma and NSCLC.[42,43] In comparison to melanoma, NSCLC, and other malignancies, BC has traditionally been considered immunologically cold, with relatively low levels of T cell infiltration and mutational burdens.[78] More recently, the immune system involvement in BC progression, response to treatment, and development of resistance are being re-evaluated, opening the door toward immunotherapeutic approaches.[41] In a recently published study, ICIs also showed promise in the treatment of metastatic BC.[79] However, there is a lack of data regarding the efficacy in BC patients with BM, as these are often excluded from clinical trials due to concerns regarding toxicities, limited efficacy of systemic agents across the BBB, and overall poor prognosis.[79,80]

For the evaluation of these 2 axes, SELP-PSGL-1 and PD-1-PD-L1, relevance to BCBM patients, we performed gene expression analysis of the GSE12276 dataset,[53] which revealed that these were overexpressed in primary tumors that relapsed to the brain, in comparison to tumors that metastasized to other organs. Additionally, IHC staining of tissue sections obtained from patients

and from our mouse models, revealed that SELP, PSGL-1, PD-1, and PD-L1 are upregulated in BCBM. In light of that, we propose these 2 axes as potential candidates for inhibiting in combination with CCL2 inhibition.

We further show that the combination of a CCL2 inhibitor with these other two immunological checkpoints is beneficial. We demonstrated this using two independent techniques: (i) syngeneic mouse models of BCBM mice, and (ii) different 3D multicellular tumoroid models.

When we tested these combinations *in vivo*, treatment with CCL2 inhibitor together with either SELP inhibitor or αPD-1 antibody led to modest improvement in some parameters compared to the monotherapies. Both combinations demonstrated an increase in OS and a slight reduction in BM volume in comparison to the relevant monotherapies. Both combination therapies also had a systemic effect, leading to a reduction in primary tumor recurrence and a reduced presentation of additional extracranial metastatic sites. As this mouse model is highly aggressive, with very large BM lesions, the most meaningful effect, which was achieved by the combined therapy of CCL2 inhibitor together with αPD-1 antibody, has prolonged the survival of mice in approximately one week, compared to the control group. Although the combination therapies had a modest improvement in some aspects of disease progression, we suggest these targets as potential combinational therapy options. Future directions should be invested in 3D *in vitro* models and mouse models for the earlier stages of micro-metastases formation, which could enable an earlier intervention and even better survival outcomes. This would also allow us to explore the cancer cell-secreted factors that initiate the activation of astrocytes in the first place and lead to the cascade of events we are describing here.

We have also tested these immunomodulation combination therapies in different 3D models, in which the drug combinations have shown a modest improvement compared to the monotherapies. In summary, due to the increased efficacy by targeting multiple axes simultaneously, and the potential to reduce acquired drug resistance incidence (though not tested), we suggest that the combination of CCL2 inhibition with (i) SELP inhibition, or (ii) PD-1/PD-L1 inhibition, upon further investigation, can be promising immunotherapeutic combination approaches.

Throughout the study, we have utilized our 3D multicellular BCBM tumor models, using two of the most common methods for fabrication of multicellular tumor spheroids:[47] (i) the hanging drop and (ii) the liquid overlay techniques. Recently, the FDA Modernization Act 2.0 was approved,

aiming to reduce animal experimentation, and to promote the development of more accurate *in vitro* models that are based on human cells, for better assessment of products for human application[81]. In comparison to traditional 2D cell culture models, 3D models composed of cancer cells and components of the TME, better mimic solid tumors regarding their architecture and phenotypical features.[47,82,83] 2D *in vitro* models do not fully represent the cellular and functional complexities of tumors.[84] On the other side of the spectrum, animal models do not only bear ethical controversy but are also limited in regard to clinically relevant responses to treatments, especially when immunotherapies are considered.[85,86] Thus, 3D models may assist in closing the gap between traditional *in vitro* and *in vivo* studies, and human clinical trials.[47]

Throughout the different steps of our study, by utilizing different 3D models, we have shown similar results regarding the effects of astrocytes on BC cells, as well as results that support the functional involvement of CCL2 in this intercommunication, while comparing to findings originated from clinical samples. In addition to cancer cells, we incorporated multiple cell populations in these models, consisting of astrocytes, endothelial cells, microglia, and PBMCs, thus better mimicking the bTME. This allowed us to perform complex studies with drugs that are not only targeting the cancer cells but also their microenvironment, with great implications for therapeutic options in humans. As an additional 3D model, we used patient-derived metastatic BC organoids, which we co-cultured with bTME components, and later treated them with the drug combinations.

In summary, we demonstrate a previously unidentified and unique requirement for the CCL2-CCR2/CCR4 axis in the crosstalk between BC cells and astrocytes during BC metastatic cascade in the brain. These data provide a new understanding of the signaling mechanisms required for brain colonization and metastatic progression. As detailed in Fig. 8, our findings implicate astrocyte-secreted CCL2 as a necessary component of the complex signaling in brain metastasis, corroborating with proinflammatory cytokines expressed on multiple immune cells, such as P-selectin on microglia/TAMs and PD-1 on T cells, presenting a unique prophylactic and therapeutic immunotherapeutic combination approach for BCBM following resection of the primary lesion.

Data availability

The authors confirm that the data supporting the findings of this study are available within the article and its supplementary material.

Acknowledgements

S.I.D. was a TEVA BioInnovation fellow in advanced research.

Funding

R.S.-F. received partial funding from the European Research Council (ERC) Advanced Grant (835227; 3DBrainStrom); and ERC Proof of Concept (PoC) Grant (862580; 3DCanPredict); The Israel Science Foundation (1969/18); The Israel Cancer Research Fund (PROF-18-682); the Morris Kahn Foundation; and La Caixa Banking Foundation Health Research BBM- Breast Cancer Brain Metastasis (HR22-00702).

Competing interests

H.B. is a consultant for AsclepiX Therapeutics, Perosphere Inc./AMAG Pharmaceuticals, Inc., StemGen, InSightec, Accelerating Combination Therapies, Camden Partners, LikeMinds, Inc., Galen Robotics, Inc., Nurami Medical, and B*CURED. **J.B.**: Advisor: AbbVie, Amgen, AstraZeneca, Bayer, MSD, Merck-Serono, Roche, Takeda; Writing/speaker engagement: BMS, Medison, Pfizer. Research funding: Immunai, OncoHost, MSD, AstraZeneca, Roche, Abbvie. **R.S.-F.** is a board director at Teva Pharmaceutical Industries Ltd., and receives unrelated research funding from Merck KGaA. All other authors report no competing interests.

Supplementary material

Supplementary material is available at *Brain* online.

References

1. Sung H, Ferlay J, Siegel RL, et al. Global cancer statistics 2020: GLOBOCAN estimates of incidence and mortality worldwide for 36 cancers in 185 countries. *CA: a cancer journal for clinicians*. 2021;71(3):209-249.

2. Siegel RL, Miller KD, Wagle NS, Jemal A. Cancer statistics, 2023. *CA: a cancer journal for clinicians*. 2023;73(1):17-48.

3. Jandial R, Hoshide R, Waters JD, Somlo G. Operative and therapeutic advancements in breast cancer metastases to the brain. *Clinical Breast Cancer*. 2018;18(4):e455-e467.

4. Custodio-Santos T, Videira M, Brito MA. Brain metastasization of breast cancer. *Biochimica et Biophysica Acta (BBA)-Reviews on Cancer*. 2017;1868(1):132-147.

5. Doron H, Pukrop T, Erez N. A blazing landscape: neuroinflammation shapes brain metastasis. *Cancer research*. 2019;79(3):423-436.

6. Witzel I, Oliveira-Ferrer L, Pantel K, Müller V, Wikman H. Breast cancer brain metastases: biology and new clinical perspectives. *Breast Cancer Research*. 2016;18(1):1-9.

7. Rostami R, Mittal S, Rostami P, Tavassoli F, Jabbari B. Brain metastasis in breast cancer: a comprehensive literature review. *Journal of neuro-oncology*. 2016;127(3):407-414.

8. Leone JP, Leone BA. Breast cancer brain metastases: the last frontier. *Experimental hematology & oncology*. 2015;4(1):33.

9. Custódio-Santos T, Videira M, Brito MA. Brain metastasization of breast cancer. *Biochimica et Biophysica Acta (BBA)-Reviews on Cancer*. 2017;

10. Joyce JA, Pollard JW. Microenvironmental regulation of metastasis. *Nature reviews cancer*. 2009;9(4):239-252.

11. Albini A, Sporn MB. The tumour microenvironment as a target for chemoprevention. *Nature Reviews Cancer*. 2007;7(2):139-147.

12. Yeini E, Ofek P, Pozzi S, et al. P-selectin axis plays a key role in microglia immunophenotype and glioblastoma progression. *Nature communications*. 2021;12(1):1-22.

13. Schwartz H, Blacher E, Amer M, et al. Incipient melanoma brain metastases instigate astrogliosis and neuroinflammation. *Cancer research*. 2016;76(15):4359-4371.

14. Valiente M, Ahluwalia MS, Boire A, et al. The evolving landscape of brain metastasis. *Trends in cancer*. 2018;4(3):176-196.

15. Pozzi S, Scomparin A, Ben-Shushan D, et al. MCP-1/CCR2 axis inhibition sensitizes the brain microenvironment against melanoma brain metastasis progression. *JCI insight*. 2022;7(17)

16. Wu S, Lu J, Zhu H, et al. A novel axis of circKIF4A-miR-637-STAT3 promotes brain metastasis in triple-negative breast cancer. *Cancer Letters*. 2024;581:216508.

17. Ferraro GB, Ali A, Luengo A, et al. Fatty acid synthesis is required for breast cancer brain metastasis. *Nature cancer*. 2021;2(4):414-428.

18. Cicero J, Trouvilliez S, Palma M, et al. ProNGF promotes brain metastasis through TrkA/EphA2 induced Src activation in triple negative breast cancer cells. *Experimental Hematology & Oncology*. 2023;12(1):104.

19. Adler O, Zait Y, Cohen N, et al. Reciprocal interactions between innate immune cells and astrocytes facilitate neuroinflammation and brain metastasis via lipocalin-2. *Nature Cancer*. 2023;4(3):401-418.

20. Xie J, Yang A, Liu Q, et al. Single-cell RNA sequencing elucidated the landscape of breast cancer brain metastases and identified ILF2 as a potential therapeutic target. *Cell Proliferation*. 2024:e13697.

21. Zou Y, Ye F, Kong Y, et al. The single-cell landscape of intratumoral heterogeneity and the immunosuppressive microenvironment in liver and brain metastases of breast cancer. *Advanced Science*. 2023;10(5):2203699.

22. Rodrigues G, Hoshino A, Kenific CM, et al. Tumour exosomal CEMIP protein promotes cancer cell colonization in brain metastasis. *Nature cell biology*. 2019;21(11):1403-1412.

23. Nicolson G, Menter D, Herrmann J, Yun Z, Cavanaugh P, Marchetti D. Brain metastasis: role of trophic, autocrine, and paracrine factors in tumor invasion and colonization of the central nervous system. *Attempts to understand metastasis formation II*. Springer; 1996:89-115.

24. Fitzgerald DP, Palmieri D, Hua E, et al. Reactive glia are recruited by highly proliferative brain metastases of breast cancer and promote tumor cell colonization. *Clinical & experimental metastasis*. 2008;25(7):799-810.

25. Zhang M, Olsson Y. Hematogenous metastases of the human brain–characteristics of peritumoral brain changes: a review. *Journal of neuro-oncology*. 1997;35(1):81-89.

26. Priego N, Zhu L, Monteiro C, et al. STAT3 labels a subpopulation of reactive astrocytes required for brain metastasis. *Nature Medicine*. 2018;24(7):1024-1035.

27. Termini J, Neman J, Jandial R. Role of the neural niche in brain metastatic cancer. *Cancer research*. 2014;74(15):4011-4015.

28. Lorger M, Felding-Habermann B. Capturing changes in the brain microenvironment during initial steps of breast cancer brain metastasis. *The American journal of pathology*. 2010;176(6):2958-2971.

29. Klein A, Schwartz H, Sagi-Assif O, et al. Astrocytes facilitate melanoma brain metastasis via secretion of IL-23. *The Journal of pathology*. 2015;236(1):116-127.

30. Daginakatte GC, Gutmann DH. Neurofibromatosis-1 (Nf1) heterozygous brain microglia elaborate paracrine factors that promote Nf1-deficient astrocyte and glioma growth. *Human molecular genetics*. 2007;16(9):1098-1112.

31. He BP, Wang JJ, Zhang X, et al. Differential reactions of microglia to brain metastasis of lung cancer. *Molecular medicine*. 2006;12(7-8):161.

32. Hoelzinger DB, Demuth T, Berens ME. Autocrine factors that sustain glioma invasion and paracrine biology in the brain microenvironment. *Journal of the National Cancer Institute*. 2007;99(21):1583-1593.

33. Roggendorf W, Strupp S, Paulus W. Distribution and characterization of microglia/macrophages in human brain tumors. *Acta neuropathologica*. 1996;92(3):288-293.

34. Markovic DS, Glass R, Synowitz M, Rooijen Nv, Kettenmann H. Microglia stimulate the invasiveness of glioma cells by increasing the activity of metalloprotease-2. *Journal of Neuropathology & Experimental Neurology*. 2005;64(9):754-762.

35. Markovic D, Vinnakota K, Chirasani S, et al. Gliomas induce and exploit microglial MT1-MMP expression for tumor expansion. *Proceedings of the National Academy of Sciences*. 2009;106(30):12530-12535.

36. Murata Ji, Ricciardi-Castagnoli P, Mange PDLE, Martin F, Juillerat-Jeanneret L. Microglial cells induce cytotoxic effects toward colon carcinoma cells: Measurement of tumor cytotoxicity with a γ-glutamyl transpeptidase assay. *International journal of cancer*. 1997;70(2):169-174.

37. Witzel I, Oliveira-Ferrer L, Pantel K, Müller V, Wikman H. Breast cancer brain metastases: biology and new clinical perspectives. *Breast Cancer Research*. 2016;18(1):8.

38. Rollins BJ. Chemokines. *Blood, The Journal of the American Society of Hematology*. 1997;90(3):909-928.

39. Marcuzzi E, Angioni R, Molon B, Calì B. Chemokines and chemokine receptors: orchestrating tumor metastasization. *International journal of molecular sciences*. 2019;20(1):96.

40. Yeini E, Ofek P, Pozzi S, et al. P-selectin axis plays a key role in microglia immunophenotype and glioblastoma progression. *Nat Commun*. Mar 26 2021;12(1):1912. doi:10.1038/s41467-021-22186-0

41. Emens LA, Adams S, Cimino-Mathews A, et al. Society for Immunotherapy of Cancer (SITC) clinical practice guideline on immunotherapy for the treatment of breast cancer. *Journal for immunotherapy of cancer*. 2021;9(8)

42. Goldberg SB, Schalper KA, Gettinger SN, et al. Pembrolizumab for management of patients with NSCLC and brain metastases: long-term results and biomarker analysis from a non-randomised, open-label, phase 2 trial. *The Lancet Oncology*. 2020;21(5):655-663.

43. Tawbi HA, Forsyth PA, Algazi A, et al. Combined nivolumab and ipilimumab in melanoma metastatic to the brain. *New England Journal of Medicine*. 2018;379(8):722-730.

44. Ferber S, Tiram G, Sousa-Herves A, et al. Co-targeting the tumor endothelium and P-selectin-expressing glioblastoma cells leads to a remarkable therapeutic outcome. *Elife*. 2017;6:e25281.

45. Rauti R, Ess A, Le Roi B, et al. Transforming a well into a chip: A modular 3D-printed microfluidic chip. *APL bioengineering*. 2021;5(2):026103.

46. Sade O, Boneberg R, Weiss Y, et al. Super-Resolution-Chip: an in-vitro platform that enables super-resolution microscopy of co-cultures and 3D systems. *Biomedical Optics Express*. 2023;14(10):5223-5237.

47. Pozzi S, Scomparin A, Dangoor SI, et al. Meet me halfway: Are in vitro 3D cancer models on the way to replace in vivo models for nanomedicine development? *Advanced Drug Delivery Reviews*. 2021;175:113760.

48. Rauh U, Wei G, Serrano-Wu M, et al. BRD-810 is a highly selective MCL1 inhibitor with optimized in vivo clearance and robust efficacy in solid and hematological tumor models. *Nature Cancer*. 2024:1-15.

49. Parida PK, Marquez-Palencia M, Ghosh S, et al. Limiting mitochondrial plasticity by targeting DRP1 induces metabolic reprogramming and reduces breast cancer brain metastases. *Nature Cancer*. 2023;4(6):893-907.

50. Sun X, Tang H, Chen Y, et al. Loss of the receptors ER, PR and HER2 promotes USP15-dependent stabilization of PARP1 in triple-negative breast cancer. *Nature Cancer*. 2023;4(5):716-733.

51. Wang L, Cossette SM, Rarick KR, et al. Astrocytes directly influence tumor cell invasion and metastasis in vivo. *PloS one*. 2013;8(12):e80933.

52. Hajal C, Le Roi B, Kamm RD, Maoz BM. Biology and models of the blood–brain barrier. *Annual Review of Biomedical Engineering*. 2021;23:359-384.

53. Bos PD, Zhang XH-F, Nadal C, et al. Genes that mediate breast cancer metastasis to the brain. *Nature*. 2009;459(7249):1005-1009.

54. Epshtein Y, Blau R, Pisarevsky E, et al. Polyglutamate-based nanoconjugates for image-guided surgery and post-operative melanoma metastases prevention. *Theranostics*. 2022;12(14):6339.

55. Ishida Y, Agata Y, Shibahara K, Honjo T. Induced expression of PD-1, a novel member of the immunoglobulin gene superfamily, upon programmed cell death. *The EMBO journal*. 1992;11(11):3887-3895.

56. Taggart D, Andreou T, Scott KJ, et al. Anti–PD-1/anti–CTLA-4 efficacy in melanoma brain metastases depends on extracranial disease and augmentation of CD8+ T cell trafficking. *Proceedings of the National Academy of Sciences*. 2018;115(7):E1540-E1549.

57. Lim SY, Yuzhalin AE, Gordon-Weeks AN, Muschel RJ. Targeting the CCL2-CCR2 signaling axis in cancer metastasis. *Oncotarget*. 2016;7(19):28697.

58. Hao Q, Vadgama JV, Wang P. CCL2/CCR2 signaling in cancer pathogenesis. *Cell Communication and Signaling*. 2020;18:1-13.

59. Jin J, Lin J, Xu A, et al. CCL2: an important mediator between tumor cells and host cells in tumor microenvironment. *Frontiers in Oncology*. 2021;11:722916.

60. Kadomoto S, Izumi K, Mizokami A. Roles of CCL2-CCR2 axis in the tumor microenvironment. *International Journal of Molecular Sciences*. 2021;22(16):8530.

61. Ling Z, Li W, Hu J, et al. Targeting CCL2-CCR4 axis suppress cell migration of head and neck squamous cell carcinoma. *Cell Death & Disease*. 2022;13(2):158.

62. Tsuyada A, Chow A, Wu J, et al. CCL2 mediates cross-talk between cancer cells and stromal fibroblasts that regulates breast cancer stem cells. *Cancer research*. 2012;72(11):2768-2779.

63. Valković T, Lučin K, Krstulja M, Dobi-Babić R, Jonjić N. Expression of monocyte chemotactic protein-1 in human invasive ductal breast cancer. *Pathology-Research and Practice*. 1998;194(5):335-340.

64. Ueno T, Toi M, Saji H, et al. Significance of macrophage chemoattractant protein-1 in macrophage recruitment, angiogenesis, and survival in human breast cancer. *Clinical cancer research*. 2000;6(8):3282-3289.

65. Saji H, Koike M, Yamori T, et al. Significant correlation of monocyte chemoattractant protein-1 expression with neovascularization and progression of breast carcinoma. *Cancer: Interdisciplinary International Journal of the American Cancer Society*. 2001;92(5):1085-1091.

66. Chavey C, Bibeau F, Gourgou-Bourgade S, et al. Oestrogen receptor negative breast cancers exhibit high cytokine content. *Breast Cancer Research*. 2007;9(1):1-11.

67. Nam J-S, Kang M-J, Suchar AM, et al. Chemokine (CC motif) ligand 2 mediates the prometastatic effect of dysadherin in human breast cancer cells. *Cancer research*. 2006;66(14):7176-7184.

68. Dutta P, Sarkissyan M, Paico K, Wu Y, Vadgama JV. MCP-1 is overexpressed in triple-negative breast cancers and drives cancer invasiveness and metastasis. *Breast cancer research and treatment*. 2018;170:477-486.

69. Fang WB, Jokar I, Zou A, Lambert D, Dendukuri P, Cheng N. CCL2/CCR2 chemokine signaling coordinates survival and motility of breast cancer cells through Smad3 protein-and p42/44 mitogen-activated protein kinase (MAPK)-dependent mechanisms. *Journal of Biological Chemistry*. 2012;287(43):36593-36608.

70. Fang WB, Sofia Acevedo D, Smart C, et al. Expression of CCL2/CCR2 signaling proteins in breast carcinoma cells is associated with invasive progression. *Scientific reports*. 2021;11(1):8708.

71. Fang WB, Yao M, Jokar I, et al. The CCL2 chemokine is a negative regulator of autophagy and necrosis in luminal B breast cancer cells. *Breast cancer research and treatment*. 2015;150:309-320.

72. Kanyomse Q, Le X, Tang J, et al. KLF15 suppresses tumor growth and metastasis in Triple-Negative Breast Cancer by downregulating CCL2 and CCL7. *Scientific Reports*. 2022;12(1):19026.

73. O'Hayre M, Salanga CL, Handel TM, Allen SJ. Chemokines and cancer: migration, intracellular signalling and intercellular communication in the microenvironment. *Biochemical Journal*. 2008;409(3):635-649.

74. Li J-Y, Ou Z-L, Yu S-J, et al. The chemokine receptor CCR4 promotes tumor growth and lung metastasis in breast cancer. *Breast cancer research and treatment*. 2012;131(3):837-848.

75. Fujimoto H, Sangai T, Ishii G, et al. Stromal MCP-1 in mammary tumors induces tumor-associated macrophage infiltration and contributes to tumor progression. *International journal of cancer*. 2009;125(6):1276-1284.

76. Bozic I, Reiter JG, Allen B, et al. Evolutionary dynamics of cancer in response to targeted combination therapy. *elife*. 2013;2:e00747.

77. Bonapace L, Coissieux M-M, Wyckoff J, et al. Cessation of CCL2 inhibition accelerates breast cancer metastasis by promoting angiogenesis. *Nature*. 2014;515(7525):130-133.

78. Gatti-Mays ME, Balko JM, Gameiro SR, et al. If we build it they will come: targeting the immune response to breast cancer. *NPJ breast cancer*. 2019;5(1):37.

79. Page DB, Beal K, Linch SN, et al. Brain radiotherapy, tremelimumab-mediated CTLA-4-directed blockade+/− trastuzumab in patients with breast cancer brain metastases. *NPJ Breast Cancer*. 2022;8(1):50.

80. Schlam I, Gatti-Mays ME. Immune Checkpoint Inhibitors in the Treatment of Breast Cancer Brain Metastases. *The Oncologist*. 2022;27(7):538-547.

81. Han JJ. FDA Modernization Act 2.0 allows for alternatives to animal testing. Wiley Online Library; 2023.

82. Datta P, Dey M, Ataie Z, Unutmaz D, Ozbolat IT. 3D bioprinting for reconstituting the cancer microenvironment. *NPJ precision oncology*. 2020;4(1):18.

83. Hickman JA, Graeser R, de Hoogt R, et al. Three-dimensional models of cancer for pharmacology and cancer cell biology: capturing tumor complexity in vitro/ex vivo. *Biotechnology journal*. 2014;9(9):1115-1128.

84. Zhou Y. Understanding the cancer/tumor biology from 2D to 3D. *Journal of Thoracic Disease*. 2016;8(11):E1484.

85. Workman P, Aboagye E, Balkwill F, et al. Guidelines for the welfare and use of animals in cancer research. *British journal of cancer*. 2010;102(11):1555-1577.

86. Mak IW, Evaniew N, Ghert M. Lost in translation: animal models and clinical trials in cancer treatment. *American journal of translational research*. 2014;6(2):114.

Figure legends

Figure 1 Astrocytes and breast cancer engage in reciprocal interactions. A-B. Proliferation rates after 96 hours, of **(A)** iRFP-labeled murine 4T1 cells, in the presence or absence of murine astrocytes (*N*=3), and **(B)** iRFP-labeled human MDA-MB-231 cells, in the presence or absence of human astrocytes (*N*=3). Data represented as fold change to time 0; Statistical significance was determined using one-way ANOVA and Dunnett's multiple comparisons test. **(C-D)** Proliferation rates after 190 hours of **(C)** murine astrocytes in the presence or absence of 4T1 conditioned medium (*N*=4), and **(D)** human astrocytes in the presence or absence of MDA-MB-231 conditioned medium (*N*=3). Data represented as fold change to time 0. **(E-F)** Quantification of tumor spheroids area after 48 hours of **(E)** mCherry-labeled 4T1 cells, in the presence or absence of murine astrocytes (*N*=5), and **(F)** mCherry-labeled MDA-MB-231 cells, in the presence or absence of human astrocytes (*N*=4). Data are presented as fold change to time 0. **(G-H)** Representative images of tumor spheroids from E-F (respectively). Scale bar = 400 μm. **(I)**

Quantification of mCherry-labeled MDA-MB-231 trans-endothelial cells, and/or trans-astrocytic migration, presented by the MDA-MB-231 mCherry signal recorded on the surface level of the transwell® membrane. Reduction in the fluorescent signal indicates the transmigration of the cells through the barrier (*N*=1). **(J)** TEER values of a barrier consisting of iPSC-derived BMEC and human pericytes, with or without human astrocytes and mCherry-labeled MDA-MB-231 measured 20 hours after the addition of MDA-MB-231 cells. Data represented as % of time 0; Statistical significance was determined using one-way ANOVA and Tukey's multiple comparisons test. **(K-L)** Illustration of the BBB models used in I-J (respectively). This image was created with BioRender.com. All data are expressed as mean ± SD; Unless otherwise stated, statistical significance was determined using an unpaired Student t-test. mAstro – murine astrocytes; hAstro- human astrocytes; BMEC- brain microvascular endothelial cells; CM- conditioned medium.

Figure 2 CCL2-CCR2/4 axis is upregulated in human and murine BCBM models and patient samples. (A-B) Cytokine arrays of media collected following 72 hours of cell culturing from mono-cultures and co-cultures of **(A)** Murine 4T1 cells and murine astrocytes (*N*=1), and **(B)** Human MDA-MB-231 cells and human astrocytes (*N*=1). Membrane negative controls were subtracted, data were normalized to membrane reference spots, and expressed per million cells. The 10 most upregulated cytokines are presented for each cell line, determined by the fold change of co-culture compared to the average of mono-cultures. Green indicates low expression, red indicates high expression. **(C-D)** CCL2/CCR2/CCR4 (red), Hoechst (blue) staining of brain metastases, primary breast cancer, adjacent/normal breast, and normal brain, in **(C)** murine tissue sections, and **(D)** human tissue sections. Scale bars = 100 μm. Representative images of selected fields (the highest expressing fields are presented). **(E-G)** Quantification of the immunostained murine tissues from C. Data are expressed as mean ± SEM; Statistical significance was determined using one-way ANOVA and Tukey's multiple comparisons tests. **(H-J)** Quantification of the immunostained human tissues from D (for H-I *N*=3, for J *n*=1-5 fields per sample). Data are expressed as mean ± SEM; Statistical significance was determined using one-way ANOVA and Tukey's multiple comparisons tests for H-I, and unpaired Student t-test for J. Dots on the graph in J represent technical repeats. **(K-M)** mRNA expression analysis of **(K)** CCL2, **(L)** CCR2, and **(M)** CCR4, on human primary breast tumors that metastasized to the brain, compared to primary tumors that metastasized to other organs. Data are presented as violin plots, with lines at the median

and quartiles; Statistical significance was determined using a one-tailed unpaired Student t-test. LCN2- Lipocalin-2; Ang1- Angiopoietin-1; PTX2- Pentraxin 2; ANG- Angiogenin; CHI3L1- Chitinase 3-like 1; Ang2- Angiopoietin-2; FLT3L- Flt-3 Ligand; CFD- Complement Factor D; mAstro – murine astrocytes; hAstro- human astrocytes; BC- breast cancer; BCBM- breast cancer brain metastases.

Figure 3 The CCL2-CCR2/CCR4 axis is upregulated in BCBM *in vitro* models. (A-B) CCL2 secretion measured by ELISA of media collected after 72 hours of cell culturing, from mono-cultures and co-cultures of **(A)** Murine 4T1 cells and murine astrocytes (*N*=3), and **(B)** Human MDA-MB-231 cells and human astrocytes (*N*=3). Data expressed as % of astrocyte secretion. **(C-D)** CCL2 mRNA expression measured by reverse transcription qPCR of RNA extracted from cancer cells and astrocytes: **(C)** 4T1 cells cultured in Astrocyte Medium (AM), Astrocyte Starvation Medium (AM 0%), or murine astrocyte CM; and murine astrocytes cultured in AM, AM 0%, or 4T1 CM (one representative out of *N*=3; dots on the graph represent technical repeats). Data expressed as fold change compared to murine astrocytes in AM. **(D)** mCherry-labeled MDA-MB-231 cells and iRFP-labeled human astrocytes, after sorting the cells by their fluorescent labeling from either mono- or co-cultures (*N*=5). Data expressed as fold change compared to human astrocytes from mono-culture. **(E-F)** FACS analysis of murine astrocytes for the intracellular CCL2 expression, following exposure to either 4T1 SFM, 4T1 SFM supplemented with LPS, or 4T1 CM. The analysis was performed for two types of astrocytic populations: **(E)** Activated / reactive astrocytes (gated for GLAST negative, GFAP positive), and **(F)** Non-GFAP-activated astrocytes (gated for GLAST positive, GFAP negative). **(G-H)** FACS analysis of 4T1 cells in murine astrocyte medium (*N*=3) of **(G)** CCR4 expression, and **(H)** CCR2 expression. (**I-J)** FACS analysis of MDA-MB-231 cells in human astrocyte medium (*N*=3) of **(I)** CCR4 expression, and **(J)** CCR2 expression. **(K-N)** Quantification of mean fluorescent intensity of cells from G-J. All data are expressed as mean ± SD. Unless otherwise stated, statistical significance was determined using one-way ANOVA and Tukey's multiple comparisons tests. mAstro – murine astrocytes; hAstro- human astrocytes; AM- astrocyte medium, AM 0%- astrocyte starvation medium (0% Fetal bovine serum (FBS)), CM- conditioned medium; SFM- serum-free medium; LPS- lipopolysaccharide.

Figure 4 The CCL2-CCR2/CCR4 axis is important for breast cancer proliferation and invasion. (A-B) Proliferation rates after 160 hours of **(A)** mCherry-labeled 4T1 cells in the presence or absence of murine astrocytes and CCL2 inhibitor bindarit (*N*=3), and **(B)** mCherry-labeled MDA-MB-231 cells in the presence or absence of human astrocytes and CCL2 inhibitor bindarit (*N*=3). Data represented as fold change to time 0. **(C-D)** Proliferation rates of **(C)** iRFP-labeled 4T1, shCCR4, or negative control sequence (shNC) cells in the presence or absence of murine astrocytes after 94 hours (one representative out of *N*=2; dots on the graph represent technical repeats), and **(D)** iRFP-labeled MDA-MB-231, shCCR4, or negative control sequence (shNC) cells in the presence or absence of human astrocytes after 72 hours (one representative out of *N*=2; dots on the graph represent technical repeats). Data represented as fold change to time 0. **(E-F)** Illustrations of the BBB models used in G, and in H-I (respectively). This image was created with BioRender.com. **(G)** TEER values of a barrier consisting of iPSC-derived BMEC and mCherry-labeled MDA-MB-231 cells, with or without the addition of recombinant CCL2 protein, measured 16 hours after the addition of MDA-MB-231 cells (*n*=3). Statistical significance was determined using an unpaired Student t-test. **(H)** TEER values of a barrier consisting of iPSC-derived BMEC, human pericytes, human astrocytes, and mCherry-labeled MDA-MB-231 cells, with or without the addition of CCL2 inhibitor bindarit, measured 20 hours after the addition of MDA-MB-231 cells (*n*=3). Statistical significance was determined using an unpaired Student t-test. **(I)** Immunostaining of a barrier consisting of iPSC-derived BMEC, human pericytes, human astrocytes, and mCherry-labeled MDA-MB-231 cells, with or without the addition of CCL2 inhibitor bindarit, or recombinant CCL2 protein, measured 20 hours after the addition of MDA-MB-231 cells. DAPI (cyan), tight junction marker ZO1 (Green), and mCherry-labeled MDA-MB-231 cells (Red). Scale bar = 20 µm. **(J-K)** Quantification of tumor spheroids area after 48 hours of **(J)** mCherry-labeled 4T1 cells, in the presence or absence of murine astrocytes and CCL2 inhibitor bindarit (one representative out of *N*=2; dots on the graph represent technical repeats); Data are presented as fold change to time 0, and **(K)** mCherry-labeled MDA-MB-231 cells, in the presence or absence of human astrocytes and CCL2 inhibitor bindarit (*N*=3); Data are presented as % of control. **(L-M)** Representative images of tumor spheroids from J-K (respectively). Scale bars = 500 µm. All data are expressed as mean ± SD; Unless otherwise stated, statistical significance was determined using one-way ANOVA and Tukey's multiple comparisons tests.

mAstro – murine astrocytes; hAstro- human astrocytes; BMEC- brain microvascular endothelial cells; CM- conditioned medium.

Figure 5 P-selectin-P-selectin ligand and PD-1-PD-L1 axes are promising candidates for immunotherapeutic combination therapy together with CCL2 inhibition. (A-D) mRNA expression analysis of **(A)** P-selectin (SELP), **(B)** P-selectin ligand 1 (PSGL-1), **(C)** Programmed death-ligand 1 (PD-L1), and **(D)** Programmed cell death protein 1 (PD-1), on human primary breast tumors that metastasized to the brain, compared to primary breast tumors that metastasized to other organs (data from GSE12276). Data are presented as violin plots, with lines at the median and quartiles; Statistical significance was determined using a one-tailed non-paired Student's t-test. **(E-F)** Quantification of tumor spheroids area after 120 hours of mCherry-labeled MDA-MB-231 cells, in the presence of human astrocytes, human microglia, and PBMCs, treated with **(E)** bindarit and\or SELPi (one representative out of *N*=3; dots on the graph represent technical repeats), and **(F)** bindarit and\or PD-L1i (*n*=4-5). Data are expressed as mean ± SD; statistical significance was determined using one-way ANOVA and Tukey's multiple comparisons tests. **(G)** Representative images of spheroids from E-F. Scale bar = 300 µm. **(H-J)** Patient-derived breast cancer liver metastasis organoids co-cultured with human astrocytes, human microglia, and PBMCs, treated with bindarit and\or SELPi, PD-L1i and Pembrolizumab. **(H)** Confocal imaging of a representative control organoid stained for CK14 antibody (Magenta), EdU-based proliferation marker (Green), and DAPI (blue). Scale bar = 50 µm. **(I)** Quantification of CK14 intensity of immunostained organoids (*n*=5 fields for each group). Data are presented as box and whiskers plot, with a line at the median and an error bar representing minimal and maximal values; statistical significance was determined using one-way ANOVA and Tukey's multiple comparisons tests. (**J)** Representative confocal images of the CK14 quantified organoids from H. CK14 (Magenta), EdU-based proliferation marker (Green). Scale bar = 200 µm. SELPi - p-selectin inhibitor; PD-L1i - programmed death-ligand 1 inhibitor.

Figure 6 Combination therapy of bindarit and either P-selectin inhibitor or αPD-1 antibody, leads to favorable outcomes in orthotopic breast cancer brain metastases mouse model. (A) Timeline (days) of primary tumor inoculation, tumor resection, metastases induction (intracranial

injection), treatments, and follow-up. **(B-C)** Kaplan-Meier survival curves of the different treatment groups. Statistical significance was determined using survival analysis of each group compared to the control group, with further adjustment of P-values using Holm-Šídák analysis. Number of mice for survival analysis: control *n*=4, bindarit *n*=6, SELPi *n*=7, αPD-1 n=6, bindarit + SELPi *n*=5, bindarit + αPD-1 *n*=6. **(D-E)** Primary tumor recurrence and extracranial metastases development inhibition are presented as the kinetics of development over time inside the groups. Number of mice for relapse analysis: control *n*=11, bindarit *n*=14, SELPi *n*=14, αPD-1 *n*=14, bindarit + SELPi *n*=14, bindarit + αPD-1 *n*=17. **(F-G)** Quantification of brain metastases size 10 days post intracranial injection. Data are expressed as mean ± SEM; statistical significance was determined using one-way ANOVA and Tukey's multiple comparisons tests. Number of mice for tumor volume analysis: control *n*=5, bindarit *n*=7, SELPi *n*=6, αPD-1 *n*=6, bindarit + SELPi *n*=7, bindarit + αPD-1 *n*=5. **(H)** Body weight change is presented as the % of change compared to the initial weight, prior to primary tumor inoculation. Data are expressed as mean ± SEM. SELPi - P-selectin inhibitor; αPD-1 – anti-programmed death-1 antibody.

Figure 7 Combination therapy of bindarit and either P-selectin inhibitor or αPD-1 antibody, leads to reduced tumor proliferation, increased immune activation, and reduced immune suppression. GFAP (red)+CCL2 (green)\CCR2 (red)\CCR4 (red)\Iba1 (red)\CD8 (red)+Caspase3 (green)\Ki67 (red)\CD31 (red)\PD-1 (red)\PD-L1 (red)\PSGL-1 (red)+SELP (green), Hoechst (blue) staining in brain metastases tissue sections from control and treated mice. Scale bars = 100 µm. Representative images of selected fields. SELPi - p-selectin inhibitor; αPD-1 – anti-programmed death-1 antibody.

Figure 8 Summary Model. Illustration showing proposed immunotherapeutic combination approach, by inhibiting breast cancer brain metastases interactions with the brain milieu. Inhibition of the 3 axes: CCL2-CCR2\CCR4, SELP-PSGL-1, PD-1-PD-L1, can prevent breast cancer brain metastases progression. By combining these treatments, favorable long-term effects could be achieved. This image was created with BioRender.com.

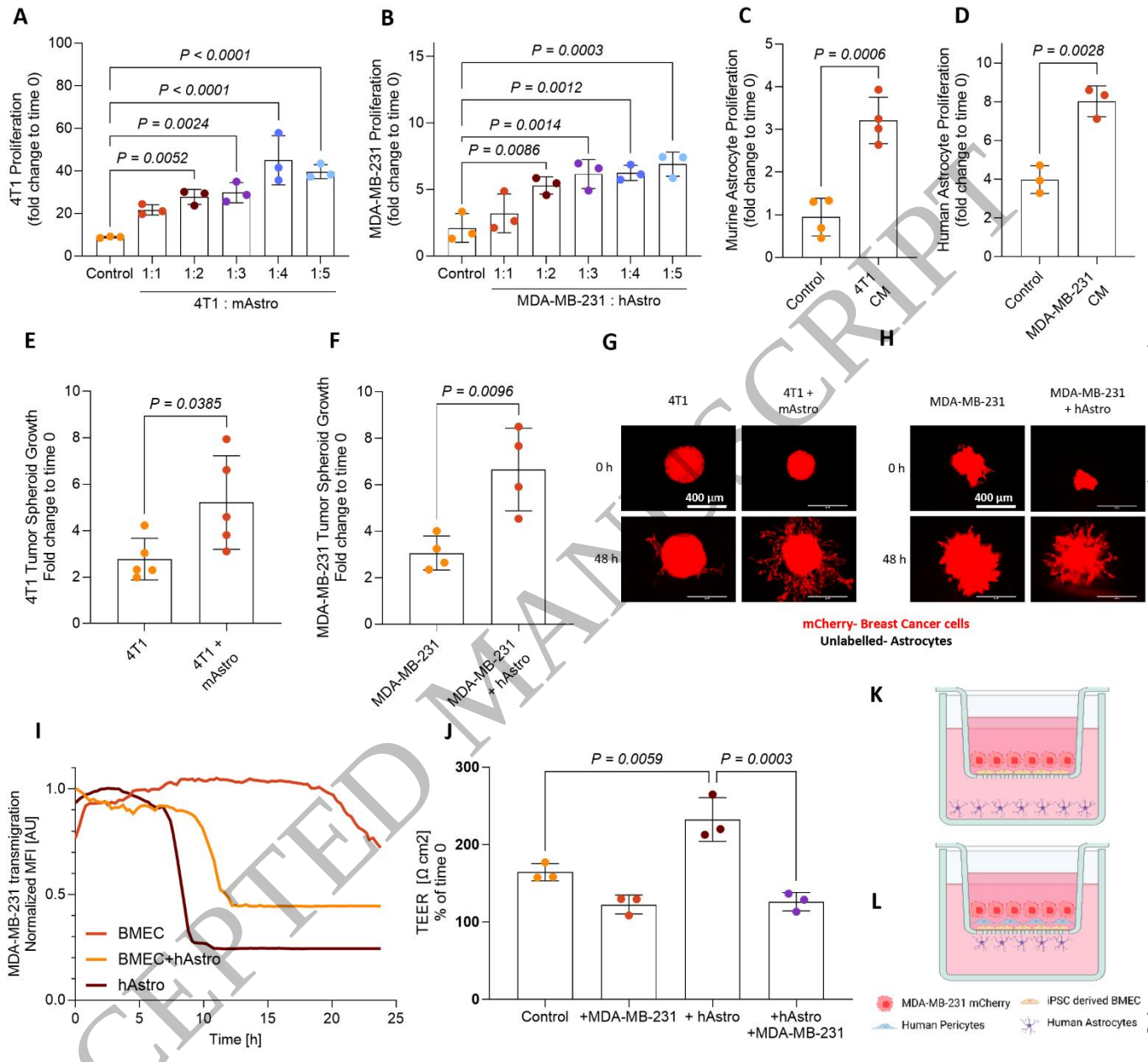

Figure 1
184x168 mm (x DPI)

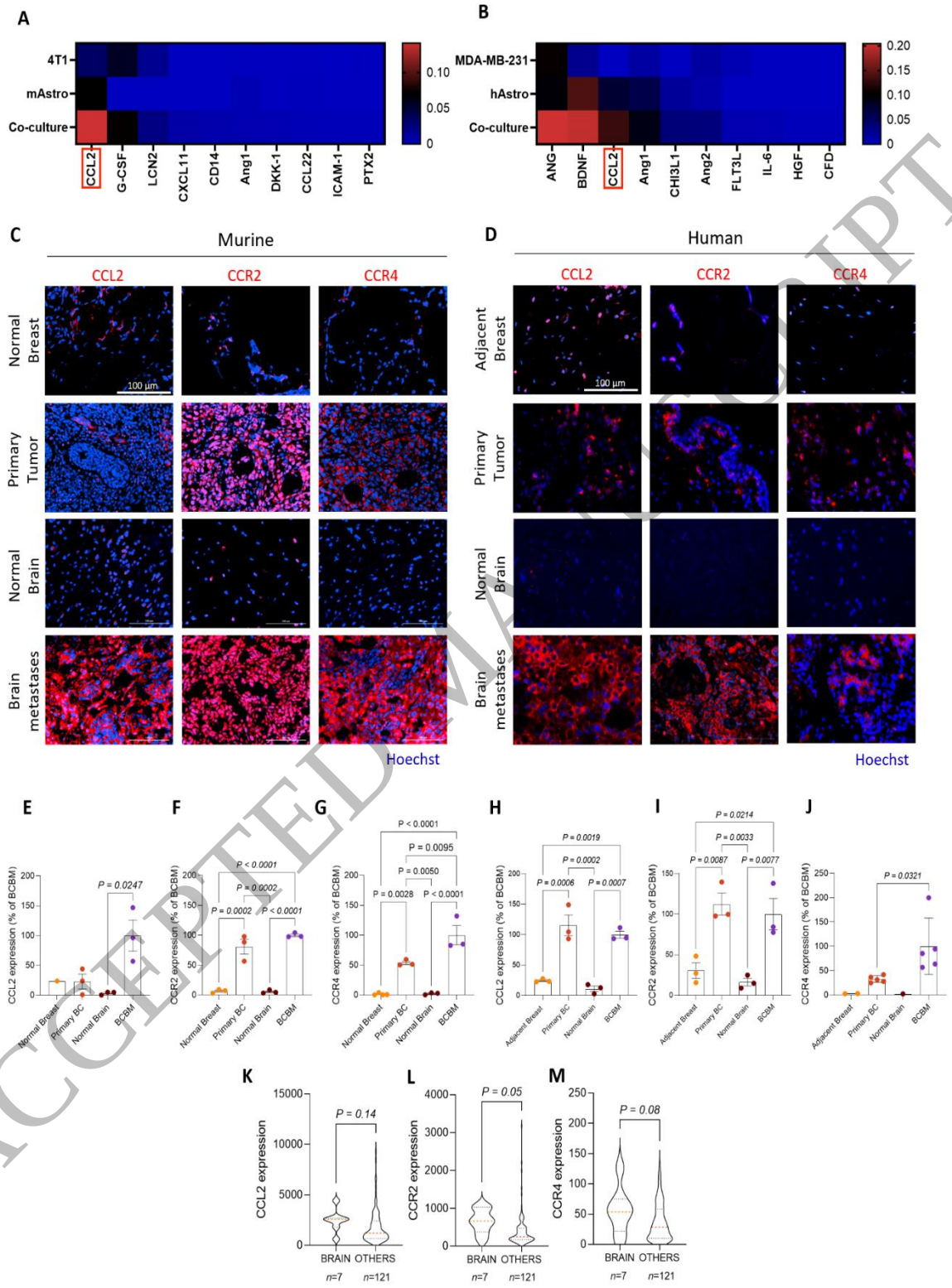

Figure 2
190x235 mm (x DPI)

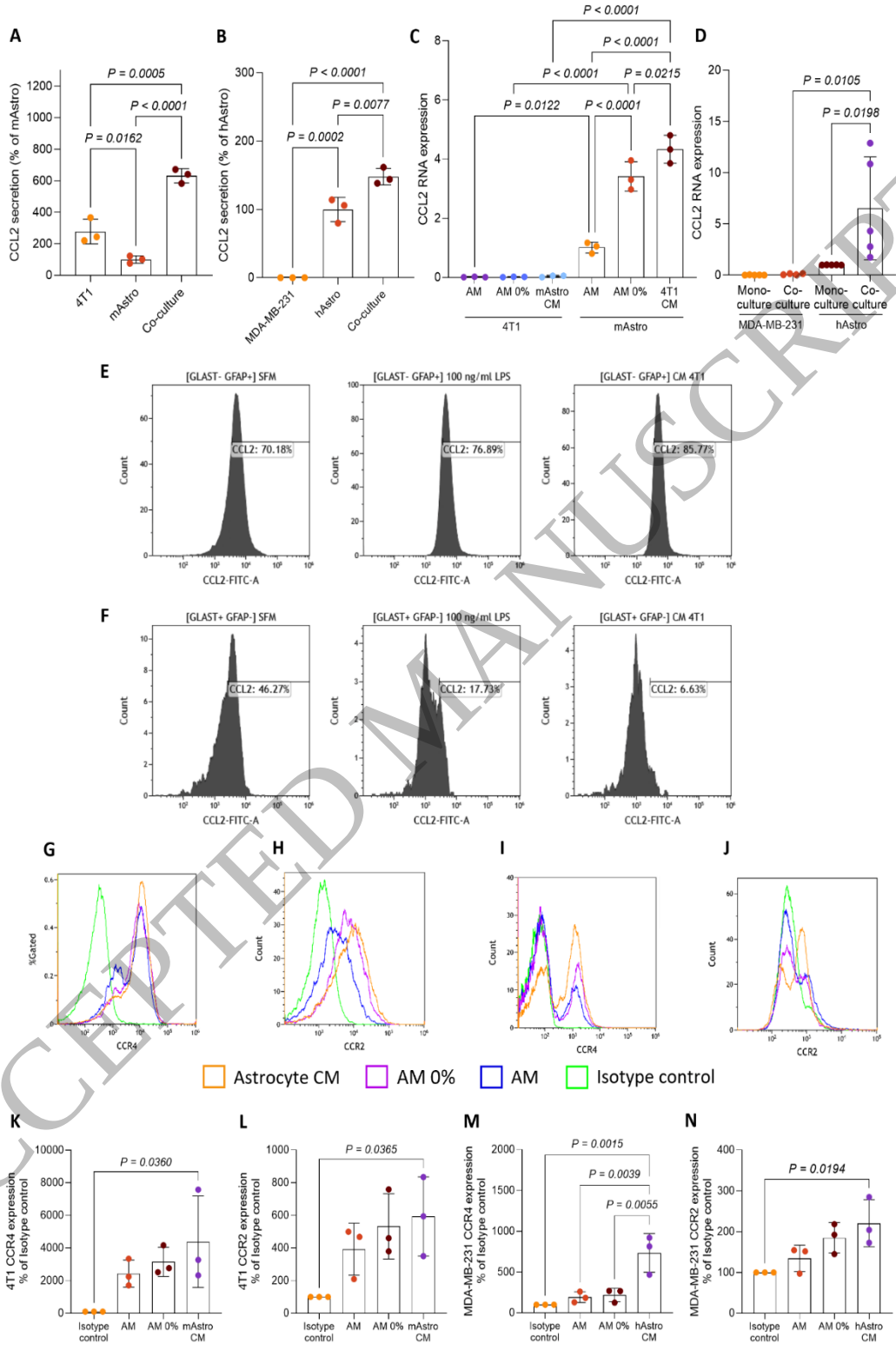

Figure 3
185x253 mm (x DPI)

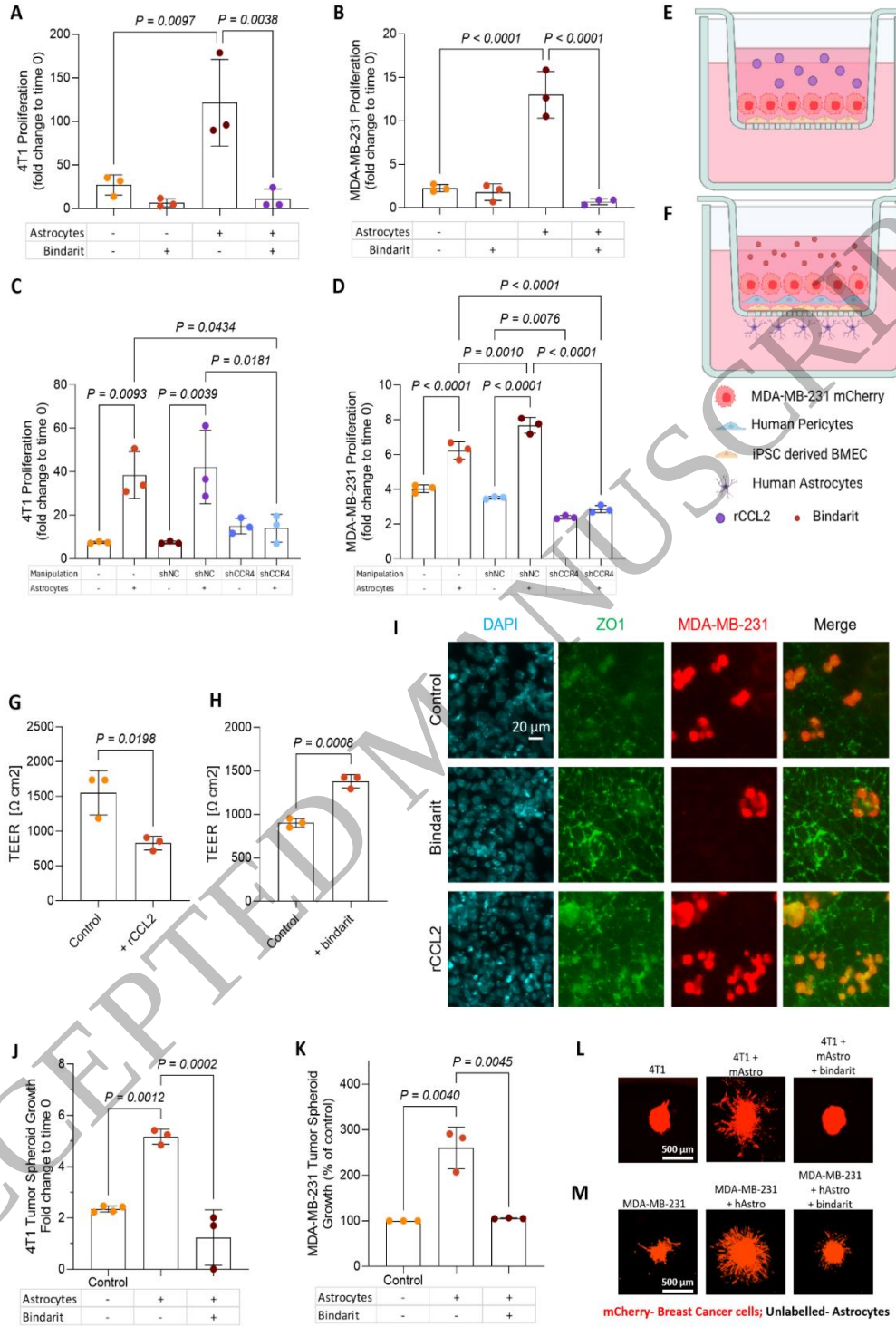

Figure 4
174x237 mm (x DPI)

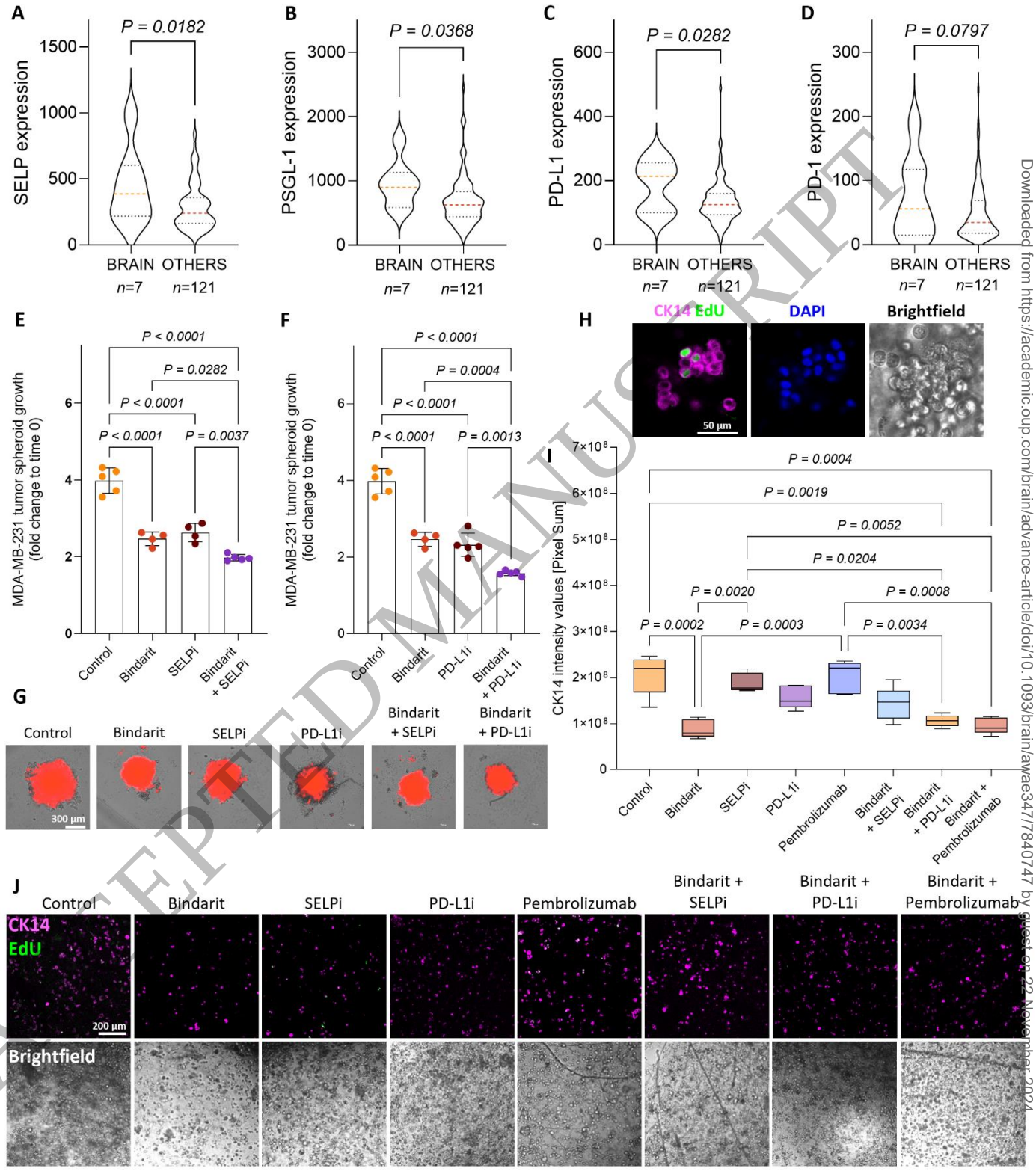

Figure 5
186x210 mm (x DPI)

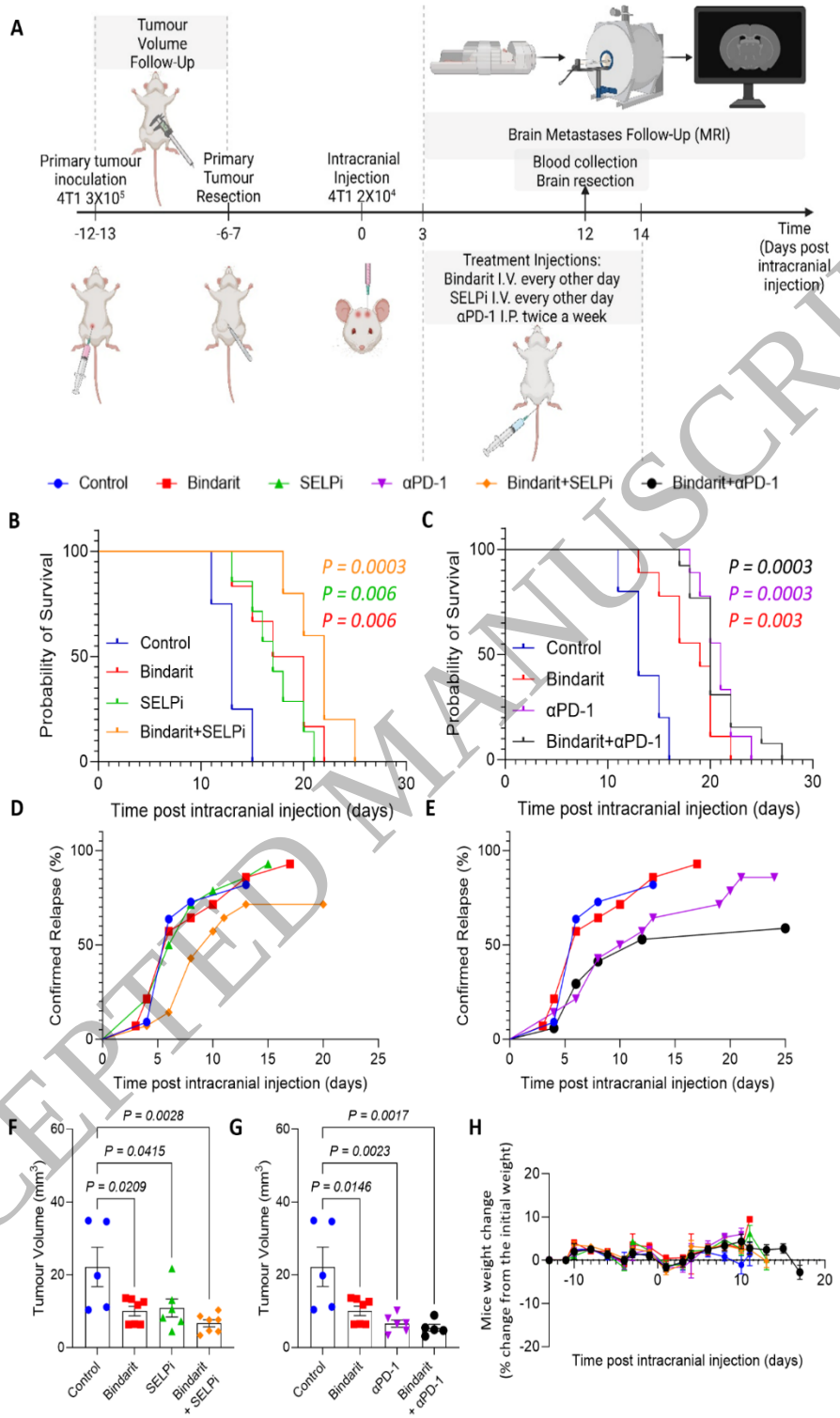

Figure 6
154x226 mm (x DPI)

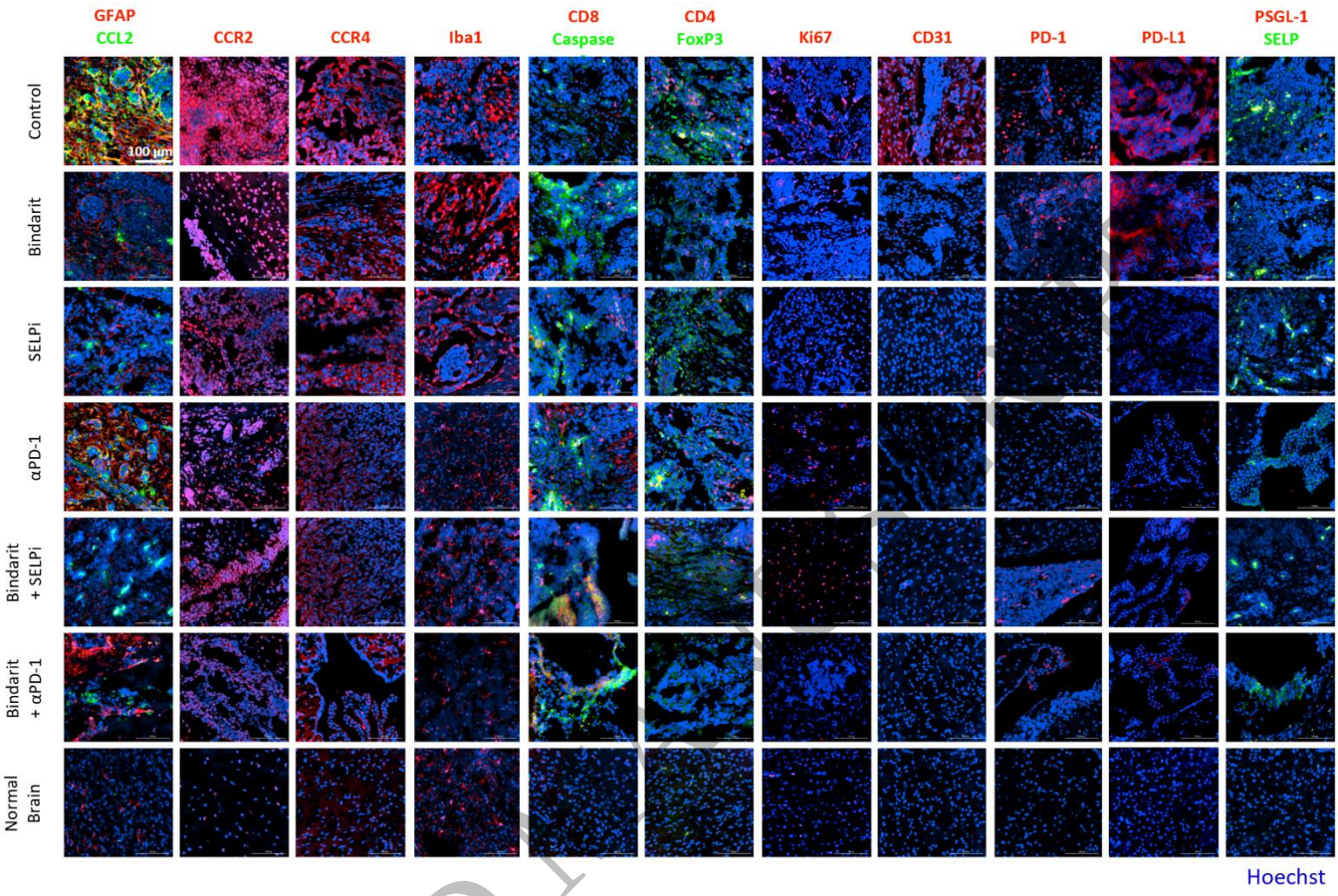

Figure 7
181x120 mm (x DPI)

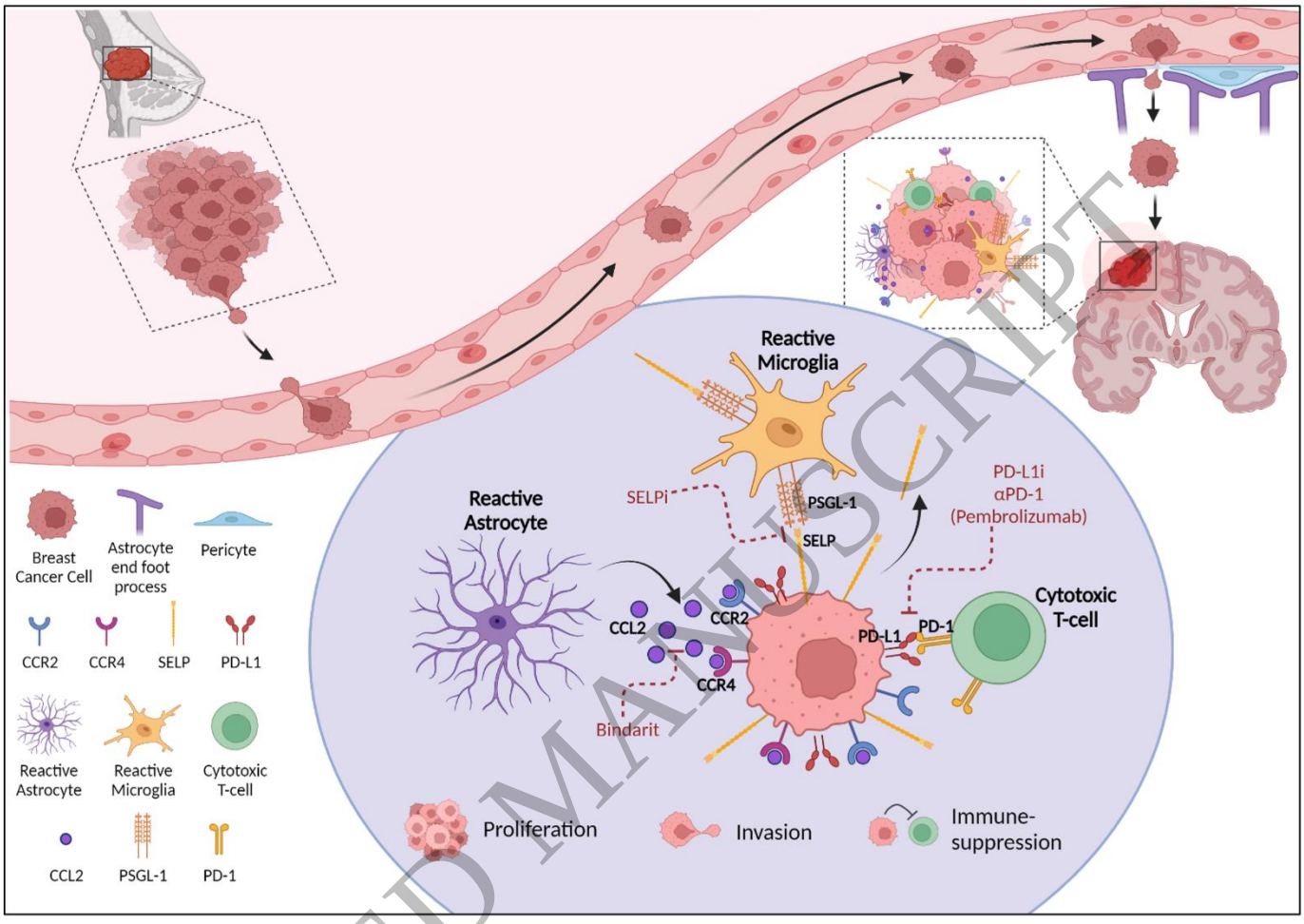

Figure 8
182x129 mm (x DPI)